IN SITU ION MICROPROBE $^{207}Pb/^{206}Pb$ DATING OF MONAZITE FROM PRECAMBRIAN METAMORPHIC SUITES, TOBACCO ROOT MOUNTAINS, MONTANA

John T. Cheney and Alexander A. Webb

Department of Geology, Amherst College, Amherst, MA 01002

Chris D. Coath and Kevin D. McKeegan

Department of Earth and Space Sciences, UCLA, Los Angeles, CA 90095.

ABSTRACT

The Precambrian rocks of the Tobacco Root Mountains have been separated into three suites: the Indian Creek Metamorphic Suite (ICMS), the Pony-Middle Mountain Metamorphic Suite (PMMMS), and the Spuhler Peak Metamorphic Suite (SPMS). The ICMS and PMMMS are quartzo-feldspathic gneiss suites that contain variable amounts of meta-supracrustal rocks. The SPMS contains primarily mafic rocks and is possibly ocean crust. Metamorphosed mafic dikes and sills (MMDS) that intruded the ICMS and the PMMMS, but not the SPMS, indicate juxtaposition of the SPMS with the other two suites after intrusion of the dikes at ~2060 Ma. All rocks have been deformed and metamorphosed together, initially at pressures greater than 1.0 GPa and temperatures greater than 750°C, followed by differential re-equilibration at ~0.6 GPa on a clockwise P-T path.

Two hundred and seventy $^{207}Pb/^{206}Pb$ spot ages of monazite grains from seventeen SPMS, five PMMMS, and eight ICMS rocks have been obtained from the UCLA ion microprobe. Based on the distribution of the ages, the samples can be divided into three groups. (1) All seventeen SPMS, one PMMMS and two ICMS samples have relatively homogeneous spot age populations that vary from ~1720 to ~1780 Ma. (2) A group of seven ICMS and PMMMS samples has spot ages from monazite grains that form an array near 2450 Ma. (3) A group of four ICMS and

PMMMS samples are bimodal in that they contain spot ages from both the 1720-1780 Ma group and the 2450 Ma array. There are younger and a few older spot ages in these samples that likely represent mixed age domains, the former between the 1720-1785 Ma and the 2450 Ma age domains and the latter between older detrital grain cores and the 2450 Ma array.

Monazite grains in the matrix have similar ages to those that occur as inclusions in garnet and kyanite. Thus, the monazite in these rocks, as well as the peak metamorphic minerals, either grew or re-equilibrated during the higher-pressure (>1.0 GPa) metamorphism. The near absence of $^{207}Pb/^{206}Pb$ ages older than 1780 Ma in the SPMS and the common occurrence of older ages in monazite from the ICMS and PMMMS are consistent with assembly of the Tobacco Root Terrane during a prolonged (60 Ma long) collision event, the Big Sky Orogeny, beginning at ~1780 Ma and culminating at ~1720Ma. The early Proterozoic Big Sky Orogeny significantly overprinted the effects of an earlier ~2450 Ma orogeny in both the PMMMS and ICMS. This older event modified pre-existing Archean rocks. However, of the 272 spot ages on monazite grains reported here, only six are significantly older than 2450 Ma and only one of these is older than 2600 Ma – a 2988 Ma spot age from a monazite inclusion in a garnet from a PMMMS sample. There is no evidence of widespread Archean events recorded in the monazite grains of the Tobacco Root Mountains.

INTRODUCTION

The Tobacco Root Mountains of Montana (Figure 8-1) have been the subject of close geologic scrutiny for over 50 years. The remarkable petrologic overview of Reid (1963) was followed by a large body of fieldwork incorporated in a number of theses from Indiana University. Vitaliano et al. (1979) summarized this work in the form of a geologic map and accompanying report. In the summer of 1993, under the leadership H. Robert Burger, one of the first Indiana University Ph.D. mappers, the attention of student geologists was once again focused on the Tobacco Root Mountains. This time the students were undergraduates working on senior projects supported by the KECK Geology Consortium. The fieldwork for some 31 undergraduate theses was completed during the summers 1993, 1995 and 1997. These projects were far ranging in scope but generally focused upon the tectonic evolution of the Tobacco Root Mountains. The resulting body of work, as developed in this book, has provided a detailed petrologic and structural framework for a complex polygenetic evolution of the Precambrian rocks comprising the area. Geochronology has been added to the growing body of knowledge most recently in the form of $^{40}Ar/^{39}Ar$ dating of hornblende and biotite (Brady et al., 200Xb) and U-Pb dating of zircon (Mueller et al., 200X). This dating has provided constraints on the age of protoliths and on the timing of cooling, but has added only limited information on the timing of the orogenic events. This chapter addresses issues of the timing of metamorphism and of the tectonic assembly of the region by providing the results of an U-Pb-Th study of monazite in rocks from the major rock suites comprising the Precambrian core of the Tobacco Root Mountains. Monazite is particularly well suited for constraining tectonic evolution because it can grow repeatedly during an orogenic cycle (Harrison et al., 2002). The purpose of this chapter is to integrate the results of our collaborative geologic work with two hundred and seventy

$^{207}Pb/^{206}Pb$ monazite spot ages acquired on the ion microprobe at the KECK Ion Microprobe Laboratory at UCLA.

BACKGROUND

Previous mapping has established the presence of three major rock units in the Tobacco Root Mountains (Figure 8-1; Figure 1-1 of Burger, 200X). In our work, as summarized in Burger (200Xa), the Precambrian rocks of the Tobacco Root Mountains have been divided into three packages: the Indian Creek Metamorphic Suite (ICMS), the Pony-Middle Mountain Metamorphic Suite (PMMMS), and the Spuhler Peak Metamorphic Suite (SPMS). The SPMS contains primarily mafic igneous rocks and may be ocean crust (Burger et al., 200X). The ICMS and PMMMS are quartzo-feldspathic gneiss suites that contain variable amounts of meta-supracrustal rocks. The ICMS is composed principally of quartzo-feldspathic gneisses and amphibolite with lesser, pelitic schist, marble, quartzite, and banded iron formation. The PMMMS is dominated by quartzo-feldspathic gneisses with lesser amounts of hornblende-plagioclase gneiss and amphibolite, but has only minor amounts of marble, quartzite, and aluminous schists and gneisses. Geochemical analysis of quartzo-feldspathic gneisses and structural observations in the ICMS and PMMMS suggest that the gneisses in the two suites may be of similar parentage (Mogk et al., 200X). One anomaly is the gedrite-bearing rocks at Cataract Mountain within the PMMMS (JBB95-39a, Figure 8-1) that occur as part of an SPMS-like sequence of aluminous schist, quartzite, quartzo-feldspathic gneiss and amphibolite. They were considered by Hanley (1975, 1976) as a possible tectonic slice of SPMS rocks in the PMMMS, an interpretation that we support in this paper.

Metamorphism

Both the ICMS and SPMS have been metamorphosed, initially at pressures exceeding 1.0 GPa (referred to as M1) and later at lower pressures of ≤ 0.6 GPa (referred to as M2). No evidence of a pre-M1 event has been found in the SPMS rocks. The ICMS/PMMMS-SPMS terrane was assembled prior to or at the time of the last ductile deformation of all the rocks because the contact is parallel to foliation within the SPMS and in the ICMS/PMMMS. The resulting structures are defined by minerals in both groups that are consistent with at least upper amphibolite facies conditions of ~ 650°C at 0.6 GPa (Harms et al., 200Xa). Because the rocks all were deformed together and both the ICMS and SPMS preserve evidence of higher-pressure metamorphism overprinted by lower-pressure metamorphism, assembly of the terrane may have occurred before or during the higher-pressure, M1 event. The mafic dikes and sills (MMDS) that intrude only the ICMS and PMMMS have been metamorphosed at the higher pressures of M1 (Brady et al., 1998). This is consistent with the 2050 Ma intrusion age and 1763 Ma metamorphic age for the MMDS as reported by Burger et al. (1999). The higher-pressure (M1) assemblages recrystallized at the relatively low pressure (≤0.6 GPa) of M2. Calculated pressures and temperatures from near rim compositions of quartz-bearing amphibolites from all three suites and the MMDS are similar. These metamorphic conditions of ~650-750°C and 0.6-0.8 GPa do not vary systematically with rock suite or geographically (Cheney et al., 200X). The textures, mineral compositions, and mineral assemblages provide constraints on the evolution of the terrane that are consistent with late tectonic denudation. This involves isobaric cooling at 800°C followed by isothermal decompression at 700°C as shown on Figure 6-21 of Cheney et al. (200X). $^{40}Ar/^{39}Ar$ spectra from amphiboles of all units yield ages of ~1710±20 Ma (Brady et al.,

200X). This requires that amphibole in all of the units cooled through the ~500°C isotherm at ca.1710 Ma.

The three different rock suites have distinctive lithologic characteristics and all three-rock suites contain some rock types with similar mineral assemblages (see Figure 6-1 of Cheney et al., 200X). In particular, all three-rock suites have aluminous gneisses and schists that contain varying amounts of biotite, sillimanite and/or kyanite, and garnet in addition to quartz, K-feldspar and/or muscovite and plagioclase. These rocks typically contain abundant monazite, are most common in the SPMS, and are least common in the PMMMS. A second important rock type that typically contains abundant monazite is the orthoamphibole (gedrite) gneiss. These rocks are common in the SPMS, rare in the ICMS, and not found in the PMMMS. In addition to gedrite, these rocks can contain varying amounts of sillimanite and/or kyanite, garnet, and cordierite.

Two orthoamphibole gneiss occurrences in the ICMS were studied: Quartz Creek (TBR-83a of Figure 8-1)) and Granite Creek (TBR-252h of Figure 8-1). These gneisses are similar to gedrite-bearing rocks that are characteristic of the SPMS, but the ICMS gedrite rocks are intercalated with BIF and typical ICMS hornblende amphibolites at both localities. The rocks at these two localities are texturally complex and contain remnant minerals from an early coarse-grained assemblage and a later, finer-grained reaction assemblage. The polymetamorphic nature of the rocks is indicated by the following observations:

- Kyanite occurs as inclusions in garnet in some orthopyroxene + orthoamphibole gneisses.
- Staurolite occurs as inclusions in kyanite and garnet.
- Coarse-grained kyanite occurs in the gedrite matrix of some orthopyroxene bearing rocks.
- Cordierite + orthopyroxene symplectite has partially replaced garnet.

- Sapphirine + spinel + cordierite symplectite has replaced aluminosilicate in silica under-saturated regions of the rocks.
- Garnet rims some orthopyroxene porphyroblasts.

Previous Geochronology

Early geochronological studies of the metamorphic rocks of Tobacco Root Mountains and adjacent ranges were based principally on K/Ar studies of micas or Rb/Sr studies of micas and whole rocks (Hayden and Wehrenberg, 1959, 1960; Giletti and Gast, 1961; Giletti, 1966, 1968). These investigators consistently found ages of 1.6-1.7 Ga, which were interpreted by Giletti (1966) as evidence of a regional metamorphism of that age. Subsequent whole rock Rb/Sr studies by Mueller and Cordua (1976) and James and Hedge (1980) yielded ages of ~ 2.7 Ga for the rocks, consistent with similar ages from elsewhere in the Wyoming Province. Both Mueller and Cordua (1976) and James and Hedge (1980) argued that they were dating the major, upper amphibolite facies metamorphism and that the earlier K/Ar work dated a less significant, greenschist facies thermal event. This view was apparently not correct, as evidence for a 2.7 Ga metamorphism has not been verified by subsequent isotopic studies in the Tobacco Root Mountains.

Recent U-Pb zircon ages from the quartzo-feldspathic gneisses of the ICMS and PMMMS have been interpreted to indicate that their igneous protoliths formed between 3.2 and 3.4 Ga (Mueller et al., 200X). This provides an upper age limit on the ICMS and PMMMS metasediments deposited upon these rocks (Harms et al., 200Xb). U-Pb ages from detrital zircons in an SPMS quartzite range in age from 3.8 down to 3.0 Ga (Mueller et al., 200X) and provide an upper age limit for the SPMS. Mueller et al. (200X) report one 2.45 Ga age from a

single subhedral zircon in this quartzite. They argue that this grain is not clearly detrital and that its subhedral shape results from metamorphic overgrowth at ~2.4 Ga. Krough et al. (1997) reported metamorphic growth of zircon at ~2.40 Ga in a PMMMS felsic gneiss that yields a primary igneous zircon age of 3.37 Ga. Roberts et al. (2002) also have reported a 2.47 Ga age based on $^{207}Pb/^{206}Pb$ step leaching of a monazite rich garnet. They have interpreted this age as a possible metamorphic event.

Evidence for a second and younger Proterozoic metamorphic event comes from the 1.77 Ga U-Pb age of zircon grains that crystallized from a melt pocket in an SPMS aluminous schist (Burger et al., 1999; Mueller et al., 2003). The 1.77 Ga date is therefore taken as the near peak age of the metamorphic event. Preliminary studies of monazite, including $^{207}Pb/^{206}Pb$ SIMS ages (Webb et al., 2001), Th-Pb SIMS ages (Cheney et al., 1999), Th-U-Pb chemical ages from the electron microprobe (Dahl et al., 1999; Dahl et al., 2002), and $^{207}Pb/^{206}Pb$ step leaching ages of garnet (Roberts et al., 2002), have yielded monazite ages between ~1.65 and 1.85 Ga. These results provide ages of metamorphic recrystallization and give further support for the existence of a younger Proterozoic metamorphic event ~1.77 Ga in age.

$^{40}Ar/^{39}Ar$ ages of 1.71 Ga of both hornblende and biotite from the Tobacco Root Mountains and adjacent Ruby Range are consistent with rapid cooling following the younger Proterozoic event (Brady et al., 200X). Roberts et al. (2002) have also recently provided $^{40}Ar/^{39}Ar$ ages from a selected subset of biotite ages that are somewhat older and average 1.76 Ga for the same area. This discrepancy is unresolved, but Brady et al. (200X) appeal to the data selection and or inter-lab errors as possible solutions.

IN- SITU I0N PROBE AGES

Sample Selection

Several hundred samples from the Tobacco Root Mountains have been examined with a petrographic microscope and with the backscattered electron detector of an SEM, both to identify the presence of monazite grains and to characterize the textural and spatial relationships of these grains. Samples were selected for dating that have monazite grains in a variety of habits such as inclusions in different metamorphic minerals (e.g. garnet, kyanite, sillimanite, and cordierite), in reaction textures typically involving the production of cordierite at the expense of garnet, and in the matrix. Samples were also selected from the same outcrops to check for consistency of results. Other samples were selected for dating to provide geographic and lithologic coverage across the terrane.

SIMS Analyses

Ion microprobe analyses of monazite were obtained from the IMS 1270 ion microprobe at the Keck National Ion Microprobe facility at UCLA. The data were acquired during three seven-day working sessions. The analytical procedures described by Harrison et al. (1995, 1997) were followed for the August, 1998 session. A similar procedure was followed in August of 1999 and December of 1999, but a different standard monazite was required in order to fully evaluate the U-Th-Pb characteristics of Tobacco Root Mountains monazite. Monazite "UCLA76" was used as standard because it has sufficient concentration of U to allow measurement of ^{238}U, $^{254}UO/^{238}U$ in addition to the normally determined masses of masses ^{232}Th, $^{264}ThO_2$, ^{238}U, $^{254}UO/^{238}U$, ^{204}Pb, ^{206}Pb, ^{207}Pb and ^{208}Pb. Although the normal protocol is to mount standard monazite grains in the same mount as the unknown monazite, the limited quantity of

UCLA76 required the use of a separate standard mount. This in turn required alternately swapping the standard and unknowns mounts in the ion microprobe sample chamber. Most of the grains analyzed during the August 1998 session were reanalyzed during August of 1999. Spear et al. (in preparation) describe additional differences between the August 1999-December 1999 sessions and the Harrison approach in some detail. In general, two calibration curves of $^{264}ThO_2/^{232}Th$ versus $^{208}Pb/^{232}Th$ and $^{254}UO/^{238}U$ versus $^{206}Pb/^{238}U$ were obtained by repeated analyses of the standard using natural instrument drift as a means of spreading out the analyses along the standard curve. During all three sessions the standard curves were built up over a seven-day session. Sample charging or instrument drift are necessary to produce spread along the standard curve and to constrain the slope of the standard curve. The calibrated values of $^{264}ThO_2/^{232}Th$, for example, for the standard should bracket those of the unknowns. The ThO_2/Th ratios do not in all cases fall with in the brackets, thus producing possible extrapolation errors on the resulting ages. A third standard curve for ($^{251}UO/^{235}U$ versus $^{207}Pb/^{235}U$) was generated by assuming that the ratio $^{238}U/^{235}U$ is 137. In this way, three independent age determinations were obtained on each spot by measurement of the three Pb isotopes ($^{208}Pb/^{232}Th$, $^{206}Pb/^{238}U$, and $^{207}Pb/^{235}U$). In addition $^{207}Pb/^{206}Pb$ ages were calculated.

Results of monazite analyses are summarized in Table 8-1. As discussed below, nearly all-spot analyses are discordant on $^{206}Pb/^{238}U$ versus $^{207}Pb/^{235}U$ concordia diagrams. Normal discordance is commonly attributed to Pb loss or mixing of ages. As the normal discordance in many cases is manifest in a line from concordia through the origin, analytic error associated with the standardization is the likely cause for this behavior (Parrish, 1990). Pb loss cannot be excluded in individual cases, especially for those ages younger than 1700 Ma. These may reflect

disturbance related to the Cretaceous Tobacco Root Batholith. In the case of either modern Pb loss or error, the $^{207}Pb/^{206}Pb$ dates are the better indicator of crystallization age.

The cause of reverse discordance is typically attributed (e.g. Parrish, 1990) to the ^{206}Pb derived from radioactive decay of ^{230}Th that was incorporated into the monazite during its growth or so called "unsupported ^{206}Pb. However, Spear et al. (in preparation) interpret the reverse discordance observed in many analyses as an analytical effect**.** This interpretation is based on the observation that the magnitude of the discordance is impossible to obtain from ^{230}Th decay given the small quantities of ^{230}Th that were likely available during monazite growth. Accordingly they argue that the most likely cause is related to sample charging on the unknown monazite that is different from that on the standard monazite. Charging that produces oxides in the plasma that are not accounted for in the standard curve produces incorrect ages. The common practice in $^{206}Pb/^{238}U$ versus $^{207}Pb/^{235}U$ studies (e.g. Wing et al., 2003) of building a standard curve over several days, from the calibration curves derived from the same standard in several different sample mounts, appears to suffer from this problem. This problem is possibly accentuated by the sample-standard swapping used in this study. Similar calibration problems may affect the $^{232}Th/^{208}Pb$ system. Because of the possible discordance in the $^{208}Pb/^{232}Th$, $^{206}Pb/^{238}U$, and $^{207}Pb/^{235}U$ systems, we use only directly measured $^{207}Pb/^{206}Pb$ ages in this paper. $^{207}Pb/^{206}Pb$ ages are independent of standard curves and, therefore, are clearly the most accurate crystallization ages for the monazite considered here. Monazite ages discussed throughout the paper are $^{207}Pb/^{206}Pb$ ages reported with 1σ (one standard error) uncertainty based on the data given in Table 8-1.

RESULTS

Results of SIMS analyses are presented in Table 8-1 and illustrated by the concordia diagrams in Figure (8-2). Histograms of age distributions for each of the three rock suites are given in individually in Figures 8-3 and collectively in Figure 8-4. The location of samples is shown on the map of the Tobacco Root Mountains in Figure 8-1. All results are reported in Table 8-1, but as discussed above, the $^{207}Pb/^{206}Pb$ ages are believed to be more consistent indicators of monaztie growth ages and are used exclusively in this study.

As shown by the histograms in Figures 8-3 and 8-4, all three-rock suites contain ages between ~1720 and ~1780 Ma, but the monazite age populations for the ICMS and PMMMS are bimodal. Both the ICMS and PMMMS suites contain a younger group of ages varying from 1720-1780 Ma and a second group of ages that form an array around ~2450 Ma.

The 272 spot ages reported in Table 8-1 were obtained from 70 different monazite grains in four different rock types among the three metamorphic suites. The most common rock types studied were aluminous gneiss, orthoamphibole gneiss, quartzo-feldspathic gneiss, and quartzite. The monazite grains selected for dating in these rocks tend to appear as equant or elongate grains reflecting end section and prismatic orientations, respectively; within a given sample the prismatic grains tend to be larger (Table 8-1). These grains range in size from less than 25 microns up to 500 microns across, but most are 100 microns across or less. The selected monazite grains vary from anhedral to euhedral, but there are no systematic trends in shape or size with regard to rock type or rock suite. Although exceptions occur, matrix grains tend to be larger than those monazite grains that occur as inclusions in other minerals.

Relationship of ages to chemical zonation of monazite grains

Spot age locations on most monazite grains and existing x-ray maps are provided in Webb (2001). Theses materials are available from the senior author and include X-ray maps for nearly all (30 of 33) of the dated ICMS and PMMMS monazite grains (see Table 8-1) as well as backscattered electron images showing the locations and values of spot ages from most of the samples reported here. Because this study evolved with the development of SIMMS techniques for monazite dating, our approach also evolved. During our initial session in June of 1998 we did not have X-ray maps of all the monazite grains prior to dating the monazite. Our initial age results and initial X-ray maps of SPMS monazite grains indicated that they are relatively homogeneous and we concentrated our efforts on the more heterogeneous monazite grains from the ICMS and PMMMS samples. However, it has become apparent that X-ray maps are essential for interpreting the ages of all monazite grains (e.g. see Williams et al., 1999; Williams and Jercinovic, 2002). Nonetheless, as shown in Table 8-1, only 12 of 37 SPMS dated monazite grains are accompanied by X-ray maps.

The available X-ray maps of the monazite grains are diverse and have varying and complex relationships among metamorphic rock suites, lithologies, and/or textural settings of the monazite grains. In some cases similar zonation patterns occur in several grains of the same sample. The distribution of Th, and Y and the geometry of their compositional variations are shown for a number of samples in Figures 8-5 through 8-11. Most of the grains are compositionally zoned, although homogenous grains exist (Figure 8-10a). Other grains, particularly in the ICMS and PMMS have irregular or patchy rims (Figure 8-8d, Figure 8-9b) or cores (Figure 8-9b, Figure 8-10d) that are especially pronounced in the Y maps. In some cases, the Y variation is inversely related to the changes in Th-U and Pb (Figure 8-11). The variation in

Pb or U (Figure 8-9) is less distinct and the elements tend to be uniformly distributed. Nd as a proxy for the rare earth elements in monazite is also evenly distributed in most samples, but there are exceptions. These features are less common in SPMS samples and the SPMS monazite tends to have simpler zonation, illustrated principally by Th variation. Some SPMS monazite grains have well defined high-Th rims (Figure 8-5), whereas others have irregular, partial high-Th rims. This relationship can be reversed, even in the same sample as shown by Figure 8-6. The weak low-Th rims in the SPMS aluminous gneiss of Figure 8-6b, the SPMS orthoamphibolite in Figure 8-7c, and the PMMMS aluminous gneiss in Figure 8-9a coupled with the irregular hi-Y cores in the ICMS aluminous schist of Figures 8-8b or with the orthoamphibole bearing rock in Figure 8-10d, illustrate that similar monazite zoning patterns can occur in rocks of differing composition and metamorphic suite.

Discerning the relationship between chemical zoning and age distribution can be difficult when the data available are limited because: 1) x-ray maps are not available for each grain; 2) some chemically zoned grains are not aged zoned and some homogenous grains have significant, but not systematic, age variation (e.g. Figures 8-8b and 8-10a); 3) we did not sample all areas of zoned grains with the ion probe beam; 4) the scale of the age variation and the chemical zoning is commonly smaller than the 20-30 micron beam of the ion microprobe and thus beyond the spatial resolution obtainable. In the context of point 3, Webb (2001) presents some high-resolution x-ray maps and exploratory electron microprobe ages provide by Mike Jercinovic at the University of Massachusetts. The higher spatial resolution of the electron microprobe permits evaluation of the small scale age variations that can occur in complex geometric configurations as reported by several workers (e.g. Williams et al., 1999; William and Jercinovic, 2002; Pyle et al., 2002; Spear and Pyle, 2002). These preliminary data coupled with existing x-ray maps that

have ion microprobe spot ages plotted on them as in Figure 8-5b indicate that the ion microprobe may be sampling different age domains in some samples. This problem is particularly exacerbated if the younger age is from relatively thin rims, as suggested in many of the x-ray maps (e.g. Figure 8-5a, Figure 8-9a-c, Figure 8-8-11a).

SPMS Monazite Ages

With six exceptions, all 137 spot ages on 37 grains from 17 SPMS samples are, within the standard error of each spot age (Table 8-1), between 1720 and 1780 Ma. The six exceptions include two younger ages that have uncharacteristically large errors, in excess of 100 Ma, and five older ages from three different samples.

The single grain spot ages vary within the standard error of each analysis in about half of the analyzed grains (Table 8-1). Typically, the spot ages of grains that exceed the spot age standard error can be related to spot location and or compositional zonation (Figure 8-5, Figure 8-6, Figure 8-7). Although there are exceptions, the older ages match up with the grain interiors whereas the younger grains, especially those less than 1730 Ma are confined to the compositionally-defined grain edges. Intermediate ages likely result from the mixing of age population in relatively large ion probe beam (see Figure 8-11a)

Most of the SPMS data are from matrix monazite grains, which have spot ages that vary from 1715±15 to 1786±6 Ma. A very limited number of the spot ages, as indicated in Table 1, are from monazite inclusions in garnet, kyanite, or biotite (Figure 8-6d); others grains occur in cordierite ± sillimanite intergrowths that have partially replaced garnet (Figure 8-5c). The inclusion ages, although very limited in number, do place upper age limits on the growth of some important minerals in these samples. With the exception of one spot age (1713±18 Ma) from a

monazite inclusion in biotite, all inclusion ages are older than ~1750 Ma. The four biotite inclusions yield ages that are older than 1753±3 Ma. Likewise the spot ages from one inclusion in garnet are older than 1771±8 Ma and those from one inclusion in kyanite are older than 1753±8 Ma. The monazite grains that occur as inclusions in cordierite, or as part of polycrystalline cordierite ± sillimanite pods that have partially replaced garnet, range in age from 1747±13 to 1786±7 Ma. Thus, spot ages younger than ~1750 Ma are restricted to matrix monazite grains in the SPMS.

The oldest age is 1920 Ma and occurs in the core of an aluminous gneiss monazite (Figure 8-6). The other four ages between 1780 and 1920 Ma may also reflect preservation of detrital cores. The 60 Ma spread (1720-1780 Ma) in SPMS ages (Figure 8-3a) is from two to six times the standard error of most of the analyses. Moreover, the single grain age variation exceeds the standard error in about half of the grains studied. Much, but not all, of this age variation can be related to compositional zoning and to the mixing of age populations in the ion probe beam. This suggests that these grains grew during multiple growth stages, or that they grew continuously over an extended period, or both. Accordingly, the spread in SPMS ages from 1720-1780 Ma represents different age populations mixing in the ion beam. But we do not know the identity or even the total number of these ages. There are a significant number of homogenous grains with a spot age near 1750 Ma. Although this 1750 ma remains problematic, the 1720-1780 span of ages represents the metamorphic growth of monazite over an extended orogenic period of some 60 Ma.

Two samples (JBB95-39a, JBB97-29c) from Cataract Mountain give only ages in the 1720-1780 Ma range. Although Cataract Mountain is surrounded by PMMMS gneisses, these rocks were identified by Hanley (1975) as very similar to the SPMS rocks of Gilmeister (1973).

The absence of monazite ages older than the 1720-1780 Ma group is consistent with Hanley's (1975) interpretation that Cataract Mountain is a possible tectonic slice of SPMS. We agree with this idea and have grouped the Cataract Mountain samples with the SPMS samples.

Finally, it is worth pointing out that the one SPMS sample collected from closest to the Tobacco Batholith contains an interesting mixed suite of ages that include a 1750±52 Ma and three $^{232}Th/^{208}$ Pb ages of 79, 74, and 76 all ±1 Ma. These young monazite grains provide a date of intrusion of the Tobacco Root Batholith. The Th-Pb ages are used here for two reasons. First, the error in the ^{207}Pb in such young rocks makes the U-Pb system unreliable. Secondly, even with very large error of ± 5% in Th-Pb due to calibration errors, the resulting error in the age would be within ±3 Ma of the intrusion age, here taken to be 76±2.5 Ma – the average of the analyses in Table 8-1.

PMMMS Monazite Ages

The bimodal age distribution shown on Figure 8-3b is from 48 spot ages of 13 monazite grains in five PMMMS samples. There are three different types of monazite age distributions from these five PMMMS samples. One sample (JBB97-27b, see Figure 1) contains monazite with ages only between 1724±6 and 1783±4 Ma, analogous to SPMS monazite. Each of the three grains in this sample is from a different textural setting (Table 8-1, Figure 8-9). Grain 1, an inclusion in a large biotite, has an irregular high-Y core and possibly a very narrow low-Y rim (Figure 8-9b). Moreover, with one unresolved exception, all of the core ages are greater than 1765±4 Ma. There is also an anomalous 1783±4 Ma spot on the grain edge. In contrast, Grain 3 is an inclusion in kyanite, but it is zoned in the opposite sense. This smaller grain (Figure 8-8d) has a low-Y core and a higher-Y rim, but the three spot ages are ~1775 Ma within error of each

other. Thus, it is tempting to equate the monazite enclosed in kyanite with at least part of the center of the monazite enclosed in the biotite grain. We have no x-ray map for monazite grain 2 from this sample. It is also relatively small (60 microns) and occurs as an inclusion in a larger matrix quartz grain. The five spot ages range from 1759±5 to 1778±6 Ma (Table 8-1), similar to the core of grain 1, the inclusion in biotite.

A second group of three samples includes 26 spot analyses from seven grains that are older than 2309 Ma. This group is somewhat heterogeneous with 17 of these older ages ranging continuously between 2425 and 2480 Ma. These ages cluster about 2450 Ma, as shown on Figure 8-3b. Five other spot ages range up in age from 2522 to 2988 Ma and are likely mixed ages between the 2450 Ma age and older remnant core ages, possibly from detrital grains. The four slightly younger spot ages that range from 2398 Ma down to 2309 Ma may also result from mixing of the 2420 Ma age, but with younger 1780 Ma ages. Most of the monazite grains from these samples are zoned, particularly in Y (similar to that in Figure 8-9) as is common in the PMMMS (described above). Unfortunately, much of this compositional variation is at a scale smaller than the ion probe beam size, resulting in the mixed spot ages.

The last type of PMMMS sample contains both the younger 1720-1780 Ma and older 2450 Ma ages. In TBR-208 (see Figure 8-1), one matrix monazite grain has only the older spot ages, whereas the other two-monazite grains contain a mixture of the younger and older ages. All three grains from this sample have complexly zoned cores and very narrow (~20 microns), low-Th rims (Figure 8-9). The low-Th rims are the source of the young ages (Figure 8-9b and Figure 8-9c). The resulting age variation in each grain reflects this zoning, especially the partial overlap between the cores and the narrow rims by the ~20-micron beam (e.g. the 1866±6 Ma rim age in

Figure 8-9c). Again the oldest spot age in this sample, 2509±16 Ma, is from a spot that partially overlaps an indistinct Y high and Th low in the grain center, possibly a detrital remnant.

ICMS Monazite Ages

Table 1 contains 87 spot ages from 20 different grains in 8 ICMS samples, 3 gedrite gneisses, and 5 aluminous gneisses. As shown on Figure 8-3c, the age distribution is similar to that of the PMMMS monazite, but there are a greater number of ages intermediate between the two peaks.

As in the PMMMS, monazite grains from two ICMS samples (two gedrite bearing rocks, from the same location) contain only the 1720-1780 Ma ages, three ICMS samples (two from the same outcrop) contain only the older spot ages, and three ICMS samples have mixed age populations. This age distribution is independent of the textural occurrence of the analyzed monazite grains because matrix grains and grains included in garnet occur in all three groups of samples. Twelve of the dated ICMS grains are from the matrix, whereas eight occur as inclusions. The youngest ages recorded by the inclusions are 1732±7 Ma from the three grains in garnet from a gedrite amphibolite, 2459±6 Ma from the two grains in garnet from aluminous gneiss, 1728±5 Ma from the single monazite in gedrite and 1977±5 Ma from one inclusion in matrix quartz from an aluminous gneiss. For comparison, matrix monazite grains range down in age to 1740±7 Ma. Spot ages from two ICMS rocks, CEH-51E (only 1720-1780 Ma ages) and TBR-83a (bimodal) are shown on Th x-ray maps in Figures 8-10 and 8-11, respectively. Both are cordierite-garnet-gedrite rocks that contain kyanite. The monazite in Figure 8-11 occurs as an inclusion in cordierite. This cordierite is texturally unique in that it occurs as coarse (1mm) subhedral grains. The Th-Y inverse compositional zoning correlates with the bimodal spot age

distribution in that the high-Th/low-Y rims are younger (~1765±13 Ma) than the cores (up to 2414±8 Ma). Most of the ion probe spots are relatively large and they overlap the compositional zones. Cordierite from other analyzed samples is much finer grained, anhedral, and confined to garnet reaction zones or symplectic intergrowths, as the case for the cordierite in sample CEH-51E (Figure 8-10c). Although the spot age variation in both grains from this sample exceeded the error of the individual analyses, only one is apparently compositionally zoned. The unzoned grain is an inclusion in garnet (Figure 8-10a-c). The spot ages vary from 1732±7 to 1760±8 Ma (Figure 8-10a) for reasons that remain unclear. The zoned monazite has a irregular core defined by high-Y and it occurs inside a large (>5mm), inclusion-riddled gedrite. The core contains spot ages that exceed 1762±5 Ma whereas the rim ages range from the overlap age of 1759±10 Ma down to 1728±5 Ma (Figure 8-10f), about the same age span as for the monazite included in garnet.

This age distribution of ICMS and PMMM samples results in part from age zoning of individual monazite grains and partly from the occurrence of only younger or older spot ages in some ICMS and PMMMS samples. The spot ages between 1790 Ma and 2450 Ma likely reflect mixing of these two or more domains in both of these suites.

DISCUSSION

There are two distinct populations of monazite spot ages from the three Tobacco Root Mountain metamorphic rock suites. This bimodal age distribution is described by a wide "peak" at 1720-1780 Ma consisting of all SPMS and some ICMS and PMMS spot ages and a second age peak near ~2450 Ma (Figure 8-4) comprised only of ICMS and PMMMS spot ages. The monazite age populations for the ICMS and PMMMS monazite grains are similar in that both are

significantly more heterogeneous than the SPMS. The heterogeneity results in part from age zoning of individual monazite grains and partly from the restricted occurrence of some ICMS and PMMMS monazite grains to either the 1720-1780 array or to the ~ 2450 array. There are younger and a few older spot ages in some ICMS and PMMMS samples that represent mixed age domains. The spot ages between 1790 Ma and 2450 Ma are from the mixing of two or more of these domains. The ages older than 2450 Ma likely represent mixtures between older remnants of detrital Archean grains and the 2450 Ma material.

The near absence of $^{207}Pb/^{206}Pb$ ages older than 1780 Ma in the SPMS and the common occurrence of these ages in monazite from the ICMS and PMMMS are consistent with assembly of the Tobacco Root Terrane during an orogenic event that began as a collision at ~1780 and continued for some 60 Ma until ~1720 Ma. We call this event the Big Sky Orogeny (Figure 8-12; see also Harms et al., 200X). We believe that this assembly involved the juxtaposition of previously unmetamorphosed SPMS and a 2450 Ma terrane consisting of the PMMMS, the ICMS, and the 2060 Ma mafic dikes and sills (MMDS). These results corroborate, extend, and clarify the preliminary findings of Webb et al. (2001), Cheney et al. (1999), Dahl et al. (1999), Dahl et al. (2002), and Roberts et al. (2002).

The distribution of $^{207}Pb/^{206}Pb$ monazite ages for the Big Sky orogeny (Figure 8-12) results from matrix grains, grains associated with cordierite – garnet reaction textures, and from monazite grains that occur as inclusion in biotite, gedrite, quartz, garnet, and kyanite. These relationships are summarized in Figure 8-13. Many of the grains in these different textural settings are compositionally zoned. The matrix monazite rains vary in age from ~1786 Ma to ~1713 Ma. The rims of the zoned matrix grains tend to yield those ages younger than ~1730 Ma. Spot ages younger than ~ 1735 Ma from Monazite inclusions in all minerals are uncommon.

Taken together these observation indicates that most of the significant mineral growth in these rocks occurred before ~ 1735 Ma, but that rims grew on matrix monazite grains between ~1735 and ~1715 Ma. Based on the spot ages from monazite inclusions in kyanite, the rocks were in the kyanite stability field and at the higher pressure of M1 until ~1750 Ma. The few SPMS and PMMMS monazite inclusions in garnet from aluminous gneisses are also older than ~1750 Ma (Figure 8-13). All of ICMS monazite inclusions in garnet are from the kyanite orthoamphibolites (see location CEH-51E of Figure 8-1). The spot ages of the monazite inclusions in these garnet grains are as young as 1732 Ma. Garnet from the aluminous gneisses likely formed during M1, but in the kyanite orthoamphibolites, garnet can grow with decreasing pressure via reactions like kyanite + gedrite = garnet + cordierite (Cheney et al., 200X) The end of garnet growth nearly coincides with the apparent end of mineral growth in other rocks of the terrane at ~1735 Ma. The Big Sky Orogeny produces partial melts and zircon growth in those melts at 1770 ±6 Ma (Mueller et al., 200X). The age of zircon crystallization and the occurrence of migmatites in aluminous gneisses are consistent with the formation of the lecosomes by muscovite dehydration melting in the kyanite stability field during M1 (Cheney et al., 200X). Initial monazite growth in aluminous rocks from many terranes is commonly coincident with the growth of garnet (Spear and Pyle, 2002). The oldest monazite ages are 1786 Ma, and precede the growth of magmatic zircon by only 15 Ma; this requires fairly rapid heating of the terrane.

Because the kyanite is demonstrably early in nearly all rocks from this terrane, the age of monazite inclusions in the kyanite significantly constrains the timing of the early high-pressure part of the Big Sky P-T-t path of Cheney et al. (200X) shown here in Figure 8-14. This clockwise path involves higher-pressure metamorphism, initially in the kyanite + orthopyroxene stability field, followed by melting at 1770 Ma in the kyanite + K-feldspar field, then nearly

isobaric cooling prior to isothermal decompression. The end of coarse-grained mineral growth at 1735 Ma coincides with isobaric cooling and the crystallization of any remaining migmatite (see Figure 8-14). The crystallizing melts would facilitate retrograde hydration reactions and could produce cordierite + biotite after garnet (Figure 8-6d). Isobaric decompression further consumes garnet in many rocks producing strong zoning in the garnet rims. The matrix monazite rims are possibly related to this decompression, which ends by 1713 Ma with further cooling.

Especially provocative is the abrupt termination of the Big Sky Orogeny as recorded by monazite ages. The lower limit of $^{207}Pb/^{206}Pb$ ages end relatively sharply in all rock suites at ~1720 Ma (Figure 8-12). This is virtually the same age as the $^{40}Ar/^{39}Ar$ cooling dates on both hornblende and biotite, at ~ 1710 Ma in these same rocks (Brady et al., 200Xb), indicative of rapid cooling of the terrane. In turn, this is remarkably consistent with tectonic denudation suggested by the P-T-t path in Figure 8-14. The coincidence of the two dating techniques both confirms the time and constrains the rapid rate of this cooling, thereby fixing the age of the end of the Big Sky P-T-t path.

The nature the 2450 Ma orogeny is not well-constrained, but there are several additional indications of a significant event in the area this time. These include the aforementioned 2450 Ma overgrowths on a 3370 Ma magmatic zircon from a PMMMS quartzofeldspathic gneiss (Krough et al., 1997) and the occurrence of ~2450 Ma ages from inherited zircon grains in the Cretaceous Tobacco Root Batholith (Figure 8-1). The 2450 Ma zircon grains have been interpreted as magmatic grains that formed in some of the material melted to make the Cretaceous magma (Mueller et al., 1998a, 1998b). We have not identified specific minerals, other than monazite or textures that are unequivocally related to the 2450 MA event. However, the metamorphosed mafic dikes and sills (MMDS) crosscut a gneissic fabric in the PMMMS and

ICMS during their intrusion at ~2060 Ma. Thus, as developed by Harms et al. (200Xb), there is a pre Big Sky fabric in the terrain and this fabric could be a remnant of the early Proterozoic orogeny at ~2450 Ma.

The Archean age of the quartzo-feldspathic basement gneisses of the PMMMS and ICMS was established from the ages of magmatic zircons from these rocks discussed in Mueller et al. (200X). These Archean basement rocks were subsequent significantly overprinted initially during the early Proterozoic at ~ 2450 Ma and subsequently during the Big Sky orogeny at 1720-1780 Ma. However, there is a limited record of Archean age monazite in the Tobacco Root Mountains. The few Archean spot ages reported in Table 8-1 are from monazite grains in metasediments of the PMMMS and ICMS, the oldest being at least ~2990 Ma, a spot age from a monazite inclusion in a garnet from a PMMMS sample. Accordingly, there is no evidence of widespread Archean events recorded in the monazite grains of the Tobacco Root Mountain region of the northern Wyoming province.

ACKNOWLEDGEMENTS

We gratefully acknowledge the use of the UCLA National Ion Microprobe Facility. We benefited greatly from the expertise and guidance of Mark Harrison. We gratefully acknowledge the remarkable hospitality and help of Marty Grove, George Jarzebinski, Liz Catlos, Jessica D'Andrea, and Steve Mojzsis. Frank Spear served as a willing lab partner and he has provided continuous and useful advice. Joe Pyle of the RPI Electron Microprobe Facility generously provided most of the x-ray maps used in this project. Mike Jercinovic of the U-Mass-Amherst Electron Microprobe Facility kindly provided additional x-ray maps on short notice. Funding for this work was provided by an Amherst College Research Award Program grant to JTC. Particular thanks go to the W. B. KECK Foundation for its continued support of the KECK Geology Consortium and undergraduate reach. Special gratitude is extended to the students and their faculty advisors who participated in the Montana KECK project. JTC is especially pleased to acknowledge the hard work and support of Montana project director H. Robert Burger, and project colleagues John B. Brady and Tekla A Harms. The manuscript has benefited immensely from excellent reviews by Frank Spear and Michael Williams and the help of John Brady.

REFERENCES CITED

Brady, J. B., Carmichael, S., Burger, H. R., Harris, C., Cheney, J. T., and Harms. T. A., 1998, Thermobarometry and geochemistry of metamorphosed mafic dikes and sills (MMDS) of the Tobacco Root Mountains, Montana: Geological Society of America Abstracts with Programs, v. 30, no. 7, p. A-97.

Brady, John B., Kovaric, Dana N., Cheney, John T., Jacob, Lisa J., and King, Jonathan T., 200X, 40Ar/39Ar Ages of Metamorphic Rocks from the Tobacco Root Mountains of Montana, in Brady, John B., Burger, H. Robert, Cheney, John T., and Harms, Tekla A., eds., Precambrian

Geology of the Tobacco Root Mountains, Montana: Geological Society of America Special Paper XXX, p. X-XX.

Burger, H. R., Brady, J. B., Cheney, J. T., Harms, T. A., Mueller, P., Heatherington, A., and Wooden, J., 1999, Evidence for a major, early Proterozoic orogenic event in the Tobacco Root Mountains of southwestern Montana: Geological Society of America Abstracts with Programs, v. 31, no. 7, p. 177-178.

Burger, H. Robert, 200X, General geology and tectonic setting of the Tobacco Root Mountains, Montana, in Brady, John B., Burger, H. Robert, Cheney, John T., and Harms, Tekla A., eds., Precambrian Geology of the Tobacco Root Mountains, Montana: Geological Society of America Special Paper XXX, p. X-XX.

Burger, H. R., H., P. W., Johnson, K. E., Tierney, K. A., Poulsen, C. J., Cady, P., Lowell, J., A., M. W., Sincock, M. J., Archuleta, L. L., Pufall, A., and Cox, M. J., 200X, General geology and geochemistry of the Spuhler Peak metamorphic suite, Tobacco Root Mountains, Montana, in Brady, J. B., Burger, H. R., Cheney, J. T., and Harms, T. A., eds., Precambrian Geology of the Tobacco Root Mountains, Montana: Special Paper XXX, Geological Society of America, p. X-XX.

Heatherington, A., and Wooden, J., 1999, Evidence for a major Early Proterozoic orogenic event in the Tobacco Root Mountains of southwestern Montana: Geological Society of America Abstracts with Programs, v. 31, no. 7, p. A177-178.

Burger, H. Robert, Peck William H., Johnson, Kathleen E., Tierney, Kara A., Poulsen, Chris J., Cady, Pamela, Lowell, Josh, MacFarlane William A., Sincock, M. Jennifer, Archuleta, LeAndra L., Pufall, Ann, and Cox, M. Jason, 200X, General Geology and Geochemistry of the Spuhler Peak Metamorphic Suite, Tobacco Root Mountains, Montana, in Brady, John B.,

Burger, H. Robert, Cheney, John T., and Harms, Tekla A., eds., Precambrian Geology of the Tobacco Root Mountains, Montana: Geological Society of America Special Paper XXX, p. X-XX

Cheney, J. T., Harms, T. A., Brady, J. B., and Burger, H. R., 1999, Early Proterozoic 208Pb/232Th in situ ion probe dating of monazite from Archean metamorphic suites, Tobacco Root Mountains, Montana: Geological Society of America Abstracts with Programs, v. 31, no. 7, p. A-178.

Cheney, John T., Brady, John B., Tierney, Kara A., DeGraff, Kathleen A., Mohlman, Heidi K., Frisch, Jessica D., Hatch, Christine E., Steiner, Michael. L., Tuit, Caroline, Steffan, Kurt J., Cady, Pamela, Lowell, Josh, Archuleta, LeAndra L., Hirst, Jillian, Carmichael, Sarah K., Fisher, Robin G. M., Wegmann, Karl W., and Monteleone, Brian, 200Xa, Proterozoic Metamorphism of the Tobacco Root Mountains, Montana, in Brady, John B., Burger, H. Robert, Cheney, John T., and Harms, Tekla A., eds., Precambrian Geology of the Tobacco Root Mountains, Montana: Geological Society of America Special Paper XXX, p. X-XX.

Dahl, P. S., Dorais, M. J., Roberts, H. J., Kelley, S. P., and Frei, R., 1999, Electron microprobe geochronometry of age-zoned monazite crystals in Archean metapelites from the Wyoming province: The nature of Pb rejuvenation and implications for regional tectonism: Geological Society of America Abstracts with Programs, v. 31, no. 7, p. A39.

Dahl, P. S., Hamilton, M. A., Terry, M. P., Roberts, H. J., Kelly, S. P., Frei, R., Jercinovic, M. J., and Williams, M. L., 2002, Comparative ion and electron microprobe dating of Wyoming province monazite, with tectonic and analytical implications: Geological Society of America Abstracts with Programs, v. 34, no. 1, p. A9.

Giletti, B. J., 1966, Isotopic ages from southwestern Montana: Journal of Geophysical Research, v. 71, p. 4029-4036.

Giletti, B. J., 1968, Isotopic geochronology of Montana and Wyoming, in Hamilton, E. I., and Farquhar, R. M., eds., Radiometric Dating for Geologists: London, Interscience Publishers, p. 111-146.

Giletti, B. J., and Gast, P. W., 1961, Absolute age of Pre-Cambrian rocks in Wyoming and Montana: Annals of the New York Academy of Sciences, v. 91, p. 454-458.

Hanley, T. B., 1975, Structure and petrology of the northwestern Tobacco Root Mountains, Madison County, Montana [Ph.D. thesis]: Indiana University, Bloomington, Bloomington, IN, 289 p.

Hanley, T. B., 1976, Stratigraphy and structure of the Central Fault Block, northwestern Tobacco Root Mountains, Madison County, Montana, in Anonymous, ed., Guidebook, The Tobacco Root Geological Society 1976 Field Conference: Butte, Montana, Special Publication 73, State of Montana Bureau of Mines and Geology, p. 7-14.

Harms, Tekla, A., Burger, H. Robert, Blednick, Daniel G., Cooper, Jacob M., King J. Toby, Owen, David R., Lowell, Josh, Sincock, Mary J., Kranenburg, Steven R., Pufall, Ann, and Picornell, Carlos M., 200Xa, Character and Origin of Precambrian Fabrics and Structures in the Tobacco Root Mountains, Montana, in Brady, John B., Burger, H. Robert, Cheney, John T., and Harms, Tekla A., eds., Precambrian Geology of the Tobacco Root Mountains, Montana: Geological Society of America Special Paper XXX, p. X-XX.

Harms, T.A., Brady, J.B., Burger, H.R., and Cheney, J.T., 200Xb: Advances in the geology of the Tobacco Root Mountains, Montana, and their implications for the history of the northern Wyoming province, in Brady, J.B., Burger, H.R., Cheney, J.T., and Harms, T.A., eds.,

Precambrian Geology of the Tobacco Root Mountains, Montana: Geological Society of America Special Paper XXX, p. X-XX

Harrison, T. M., KcKeegan, D. D. & Le Fort, P. (1995). Detection of inherited monazite in the Manaslu leucogranite by $^{208}Pb/^{232}Th$ ion microprobe dating: Crystallization age and tectonic implications. Earth and Planetary Science Letters, 133, 271-282.

Harrison, T. M., Ryerson, F. J., Le Fort, P., Yin, A., Lovera, O. M. & Catlos, E. J. (1997). A Late Miocene-Pliocene origin for the Central Himalayan inverted metamrophism. Earth and Planetary Science Letters, 146, 1-7.

Harrison, T. M, Catlos, E.J. and Montel, J.M. (2002) U-TH-Pb Dating of Phosphate Minerals. In M.J. Kohn, J. Rakovan, and J.M. Hughes, Eds. Phosphates: Geochemical, Geobiological, and Materials Importance, 48, p. 337-362. Reviews in Mineralogy and Geochemistry, Mineralogical Society of America, Washington, D. C.

Hayden, R. J., and Wehrenberg, J. P., 1959, Potassium-argon dating in western Montana: Geological Society of America Bulletin, v. 70, no. 12, Part 2, p. 1778-1779.

Hayden, R. J., and Wehrenberg, J. P., 1960, A (super 40) -K (super 40) dating of igneous metamorphic rocks in western Montana: Journal of Geology, v. 68, no. 1, p. 94-97.

James, H. L., and Hedge, C. E., 1980, Age of the basement rocks of Southwest Montana: Geological Society of America Bulletin, v. 91, no. 1, p. 111-115.

Krogh, T. E., Kamo, S., and Hess, D. F., 1997, Wyoming province 3300+ gneiss with 2400 Ma metamorphism, northwestern Tobaco Root Mountains, Madison Co., Montana: Geological Society of America Abstracts with Programs, v. 29, no. 6, p. A-408.

Mogk, D. W., Burger, H. R., Wooden, J. L., D'Arcy, K., Heatherington, A. L., and Abeyta, R. L., 2003, Geochemistry of Quartzofeldspathic Gneisses and Metamorphic Mafic Rocks of the Indian Creek and Pony-Middle Mountain Metamorphic Suites, Tobacco Root Mountains,

Montana, in Brady, J. B., Burger, H. R., Cheney, J. T., and Harms, T. A., eds., Precambrian Geology of the Tobacco Root Mountains, Montana: Special Paper XXX, Geological Society of America.

Mueller, P. A., and Cordua, W. S., 1976, Rb-Sr whole rock age of gneisses from the Horse Creek area, Tobacco Root Mountains, Montana: Isochron West, no. 16, p. 33-36.

Mueller, P., Heatherington, A., Wooden, J., Mogk, D., and Bowes, D., 1998a, The Wyoming province and its place in the evolution of Precambrian North America: Geological Society of America Abstracts with Programs, v. 30, no. 7, p. A-46.

Mueller, P. A., Wooden, J. L., Nutman, A. P., and Mogk, D. W., 1998b, Early Archean crust in the northern Wyoming province: evidence from U-Pb ages of detrital zircons: Precambrian Research, v. 91, p. 295-307.

Mueller, Paul A., Burger, H. Robert, Heatherington, Ann, Wooden, Joseph, Mogk, David W., and D'Arcy, Kimberly, 200X, Age and Evolution of the Precambrian Crust, Tobacco Root Mountains, Montana, in Brady, John B., Burger, H. Robert, Cheney, John T., and Harms, Tekla A., eds., Precambrian Geology of the Tobacco Root Mountains, Montana: Geological Society of America Special Paper XXX, p. X-XX.

Parrish, R. (1990). U-Pb dating of monazite and its application to geological problems. Canadian Journal of Earth Sciences, v. **27**, p. 1431-1450.

Pyle, J.M., Spear, F.S., and Wark, D.A. (2002) Electron microprobe analysis of REE in apatite, monazite, and xenotime: Protocols and pitfalls. In M.J. Kohn, J. Rakovan, and J.M. Hughes, Eds. Phosphates: Geochemical, Geobiological, and Materials Importance, 48, p. 337-362. Reviews in Mineralogy and Geochemistry, Mineralogical Society of America, Washington, D. C.

Reid, R. R., 1963, Metamorphic rocks of the northern Tobacco Root Mountains, Madison County: Geological Society of America Bulletin, v. 74, p. 293-306.

Roberts, H.J., Kelley, S.P., Dahl, P.S., and Frei, R. 2002. New ^{207}Pb–^{206}Pb and ^{40}Ar–^{39}Ar ages from SW Montana, USA: constraints on the Proterozoic and Archæan tectonic and depositional history of the Wyoming Province. Precambrian Research v. 117 p. 119–143.

Spear, F.S., and Pyle, J.M. (2002) Apatite, monazite, and xenotime in metamorphic rocks. In M.J. Kohn, J. Rakovan, and J.M. Hughes, Eds. Phosphates: Geochemical, Geobiological, and Materials Importance, 48, p. 293-335. Reviews in Mineralogy and Geochemistry, Mineralogical Society of America, Washington, D. C.

Spear,F.S., Cheney, J.T., Pyle, J.M., Harrison,T.M. And Lane, G. In review, Monazite geochronlogy on a transect across central New England. MS 31 pages and 30 figures.

Vitaliano, C. J., Burger, H. R., Cordua, W. S., Hanley, T. B., Hess, D. F., and Root, F. K., 1979a, Geologic map of southern Tobacco Root Mountains, Madison County, Montana: Geological Society of America Map and Chart Series MC-31, scale 1:62,500.

Webb, A.A., Cheney, J.T. Harms, T.A. and Coath, C.D., 2001, $^{207}Pb/^{206}Pb$ ion microprobe dating of monazite from Precambrian metamorphic suites, Tobacco Root Mountains, southwestern Montana. Geological Society of America, Abstracts with Programs, V33, no.1, p. A10.

Webb, A.A., Ion microprobe dating of monazite from Precambrian metamorphic suites, Tobacco Root Mountains, Montana [B.A., thesis]: Amherst College, 99 p.

Williams, M.L., Jercinovic, M.J., and Terry, M.P., 1999, Age mapping and dating of monazite on the electron microprobe: Deconvoluting multistage tectonic histories: Geology, v.27, no.11, p.1023-1026.

Williams, M.L. and Jercinovic, M. J., 2002, Microprobe Monazite Geochronology: Putting Absolute Time into Microstructural Analysis. Journal of Structural Geology, v.24, p. 1013-1028.

Wing, B. A., Ferry, J. M. and Harrison, T. M., 2003, Prograde destruction and formation of monazite and allanite during contact and regional metamorphism of pelites: petrology and geochronology. Cont. Min. Pet., v.145, p. 228-250.

FIGURE CAPTIONS

Figure 8-1. Generalized geologic map of the Tobacco Root Mountains (modified from Burger, 2003) showing the distribution of dated samples and the metamorphic rock suite of each dated sample. The quartzo-feldspathic gneiss unit to the north and east of the SPMS has been designated the PMMMS whereas the rocks to the south and west of the SPMS are referred to as the ICMS. The PMMMS-ICMS boundary is marked with a thick dashed line dashed line. The geographic outline of the Tobacco Root Mountains is shown by the 5000 foot contour.

Figure 8-2. Representative concordia plots for spot ages by metamorphic rock suite: (a) SPMS, (b) PMMMS and (c) ICMS. Error ellipses are one sigma.

Figure 8-3. Histograms showing $^{207}Pb/^{206}Pb$ spot age distribution by metamorphic rock suite: (a) SPMS, (b) PMMMS, (c) ICMS. The bin size on all three diagrams is 10Ma.

Figure 8-4. Histogram showing the distribution of spot ages from all three metamorphic rock suites. The bin size 10 Ma. .

Figure 8-5. Monazite images from grain 9 of sample TBR-129, an aluminous gneiss from the SPMS. Backscattered image (a) and x-ray maps illustrating systematic Th (b) and Pb (a) and week Y compositional zoning of monazite grains. (b) Th x-ray map showing ion microprobe spot locations and $^{207}Pb/^{206}Pb$ ages for grain 1. (c) and (d)Photomicrographs showing textural setting of grain 9 in sillimanite fibers in a moat of cordierite (darker gray) after garnet reaction zone.

Figure 8-6. Monazite images from grain 2 of sample TBR-129, an aluminous gneiss from the SPMS. (a) Backscattered image and x-ray maps illustrating showing very weak inverse Y and Th compositional zoning.(b) BSE image showing ion microprobe spot locations and $^{207}Pb/^{206}Pb$ ages for grain 2. (c) and (d) Photomicrographs showing textural setting grain 2 as inclusion in coarse-grained biotite that grew from back reaction of melt during cooling. Note the many garnet fragments enclosed in the biotite.

Figure 8-7. Monazite images from sample TBR-16, an orthoamphibole gneiss from the SPMS. (a),(b), and (c) show $^{207}Pb/^{206}Pb$ spot age locations and x-ray maps for grains 1, 2 and 3 respectively.

Figure 8-8. Monazite images from sample JBB-27b, an aluminous gneiss from the PMMMS. (a) Th x-ray map (b) Y x-ray map shows the spot age locations and Y zoning of grain 1. (c) The ion probe pits and he textural setting of grain 1 in the matrix enclosed by coarse biotite laths. (d),(e) and (f) show the $^{207}Pb/^{206}Pb$ spot age locations and x-ray maps for grain 2, an inclusion in kyanite as shown in (g) and (h). Note that the high Y rim is the opposite of the zoning for grain 1which has a high Y core.

Figure 8-9. Monazite images from sample TBR-208, also an aluminous gneiss from the PMMMS. (a),(b) and (c) show the spot age locations and x-ray maps for grains a, b and c, respectively. The accompanying photomicrographs show ion probe pits and the setting of the three grains in the matrix. The straight white stripes in the photomicrographs are scratches in the

gold coating. Note the thin low Th and high Y discontinuous rims on these grains and the younger ages that are from this rim in (b) & (c). The younger ages are from ion probe spots that seem to overlap the chemical zoning.

Figure 8-10. Monazite images from sample CEH-51e, an orthoamphibole gneiss from the ICMS. (a) Shows the $^{207}Pb/^{206}Pb$ spot ages and the inset shows the compositional homogeneity of grain 1. The small white circles show the analyses locations on the Th x-ray map. (b) and (c) show the euhedral monazite as an inclusion in garnet. A cordierite-orthopyroxene symplectite has developed during decompression on the edge of the garnet. (d) shows an irregular core with high Th and low Y in grain 3, a matrix monazite that is largely enclosed in gedrite as shown in (e). (The spot ages from grain 3 are shown in (f)

Figure 8-11. Monazite images from sample TBR-83a, an orthoamphibole gneiss from the ICMS. (a) Shows the systematic relationship between spot ages and the inverse variation of Th and Y . This set of figures again illustrates the potential overlap of some ion microprobe spots and the chemical zoning. (b) Provides the textural setting of this grain as an inclusion in cordierite.

Figure 8-12. Enlarged histogram showing the distribution of Big Sky $^{207}Pb/^{206}Pb$ spot age spot ages for all three metamorphic rock suites. The bin size is 10 Ma

Figure 8-13. Summary of $^{207}Pb/^{206}Pb$ sot ages from monazite grains by textural setting. The gray boxes outline the range of ages for each of the monazite textures as : (1)inclusions in garnet, kyanite, gedrite, biotite or quartz, (2) in cordierite- garnet reaction zones and (3) in the matrix.

The range of ages from monazite matrix rims is also shown. Within each box, the range of ages is indicated for samples from each metamorphic rock suite, SPMS by the solid line, ICMS by the short dashes and PMMMS by the longer dashes.

Figure 8-14. Summary diagram, modified from Figure 6-21 of Cheney et al 200X, showing timing constraints on the P-T-t evolution of the metamorphic rocks from the Tobacco Root Mountains during the 1.78-172 Ga Big Sky Orogeny. The P-T path is shown by the heavy black line. Specific fields outlined on the diagram are: (1) the lower part of the stability field of kyanite + orthopyroxene, (2) the lower part of the stability field of kyanite + K-feldspar produced by dehydration melting from Spear et al. (1999), (3) the range of temperatures and pressures (dark oval) calculated from the garnet-hornblende-plagioclase-quartz thermobarometer (4) calculated pressures and temperatures from garnet-othopyroxene equilibria field (rectangular box) from the orthopyroxene-cordierite symplectite, (5) a calculated decompression path (wide arrow) resulting from cordierite growth based on observed Mn-zoning of garnet (6) the upper stability of staurolite + quartz (dashed line) and (7) a dehydration melting curve for amphibolite. The details of these constraints are provided in figure 6-21 of Cheney et al. (200X).

TABLE 1: Ion Microprobe Ages of Monazites from the Tobacco Root Mountain, Montana																	
Sample/Grain/Spot#	Date	Grain Size	Grain	Textural	Xray-map	Age (Ma)	1 s.e.	Age (Ma)	1 s.e.	Age (Ma)	1 s.e.	Age (Ma)	1 s.e.	Th O2/	diogenic	diogenic	diogenic
		microns	Shape*	Setting	X=Map	207Pb/	207Pb/	208Pb/	208Pb/	206Pb/	206Pb/	207Pb/	207Pb/	Th	208Pb	207Pb	206Pb
						206Pb	206Pb	232Th	232Th	238U	238U	235U	235U				
						**	***		***		***		***				
ICMS																	
TBR-252	**Granite Creek**	**ICMS**	**thoamphibole Gneiss**														
TBR252H_g1s1	1999-08-16Aug	150	E/A	in Garnet	X	1766	8	1821	10	1941	15	1858	8	6.26	99.86	99.14	99.9
TBR252H_g1s2	1999-08-16Aug					1826	25	1976	265	2011	242	1922	127	5.58	99.73	98.21	99.79
TBR252H_g1s3	1999-08-16Aug					1797	35	1739	44	1765	60	1780	30	6.50	99.43	96.45	99.58
TBR252H_g1s4	1999-08-16Aug					1827	17	1847	18	1922	20	1877	14	6.62	99.79	98.34	99.8
TBR252H_g1s5	1999-08-16Aug					1745	17	1769	32	1769	38	1758	21	6.32	99.04	94.3	99.32
TBR252H_g1s6	1999-08-16Aug					1810	37	1643	34	1872	48	1843	25	7.06	99.54	96.41	99.57
TBR252H_g1s7	1999-08-16Aug					1777	17	1683	22	1835	33	1808	20	6.24	99.93	99.53	99.95
TBR-252h_Mon1_pt1	98_08_28aug			same as grain 1		1747	3	1631	7					4.02			
TBR-252h_Mon1_pt2	98_08_28aug					1760	3	1703	25					3.19			
TBR-252h_Mon1_pt3	98_08_28aug					1757	6	1292	24					3.21			
TBR252H_g2s2	1999-08-16Aug	75	E	in Garnet	X	1743	5	1825	13	1799	15	1773	8	5.98	99.94	99.79	99.98
TBR252H_g2s3	1999-08-16Aug					1746	14	1715	22	1737	27	1741	15	5.50	99.95	99.69	99.96
TBR252H_g2s4	1999-08-16Aug					1755	17	1662	39	1755	40	1755	22	4.90	99.89	99.46	99.94
TBR252H_g2s5	1999-08-16Aug					1741	12	1786	26	1858	24	1804	12	5.54	99.82	99.29	99.92
TBR252H_g2s6	1999-08-16Aug					1747	11	1729	16	1857	19	1806	8	5.77	99.87	99.4	99.93
TBR-252h_Mon2_pt1	98_08_28aug			same as grain 2		1765	4	1740	12					3.67			
TBR-252h_Mon2_pt3	98_08_28aug					1766	5	1773	39					3.00			
TBR-252h_Mon2_pt2	98_08_28aug					1759	3	1704	32					2.87			
TBR-252h_Mon2_pt4	98_08_28aug					1762	4	1421	61					2.37			
						1754	**10**										
CEH-51	**Granite Creek**	**ICMS**	**thoamphibole Gneiss**														
CEH51_g1s1	1999-08-17Aug	250	P	in Garnet	X	1736	10	1674	8	1772	9	1755	7	6.94	99.87	99.22	99.91
CEH51_g1s2	1999-08-17Aug					1732	7	1707	9	1782	17	1759	8	7.83	99.83	99.67	99.96
CEH51_g1s3	1999-08-17Aug					1750	7	1694	9	1769	12	1760	8	7.54	99.85	99.72	99.97
CEH51_g1s4	1999-08-17Aug					1759	6	1714	9	1783	12	1772	7	7.27	99.79	99.59	99.95
CEH51_g1s5	1999-08-17Aug					1760	8	1698	8	1782	12	1772	6	7.14	99.89	99.29	99.92
CEH-51b_sp1	98_08_26Aug\			same as grain 1		1749	9	1638	14					4.87			
CEH-51b_sp2	98_08_26Aug\					1739	4	1642	13					4.92			
CEH-51b_sp3	98_08_26Aug\					1738	6	1653	13					4.85			
CEH-51b_sp4	98_08_26Aug\					1735	11	1667	12					4.67			
CEH-51b_sp5	98_08_26Aug\					1744	11	1590	10					4.47			
						1744	**10**										
CEH51_g2s1	1999-08-17Aug	160	E/A	in Gedrite	X	1750	10	1580	10	1662	16	1701	10	5.77	99.91	99.05	99.89
CEH51_g2s2	1999-08-17Aug					1762	5	1667	12	1722	14	1740	8	5.60	99.86	99.53	99.95
CEH51_g2s3	1999-08-17Aug					1738	7	1711	16	1792	19	1767	10	5.22	99.87	98.64	99.85
CEH51_g2s4	1999-08-17Aug					1766	10	1594	15	1725	22	1743	12	5.43	99.88	99.31	99.92
CEH51_g2s5	1999-08-17Aug					1749	8	1656	15	1752	21	1751	12	5.34	99.93	99.28	99.92
CEH51_g2s6	1999-08-17Aug					1728	5	1607	22	1720	25	1724	14	4.71	99.88	99.23	99.91
						1749	**14**										
ceh-51e_sp1	98_08_26Aug\	?		?		1815	47	1260	47					5.49			
ceh-51e_sp1@1	98_08_26Aug\					1743	16	1764	33					3.71			

Sample/Grain/Spot#	Date	Grain Size	Grain	Textural	Xray-map	Age (Ma)	1 s.e.	Age (Ma)	1 s.e.	Age (Ma)	1 s.e.	Age (Ma)	1 s.e.	Th O2/	diogenic	diogenic	diogenic
		microns	Shape*	Setting	X=Map	207Pb/	207Pb/	208Pb/	208Pb/	206Pb/	206Pb/	207Pb/	207Pb/	Th	208Pb	207Pb	206Pb
						206Pb	206Pb	232Th	232Th	238U	238U	235U	235U				
						**	***		***		***		***				
TBR-83	**Quartz Creek Ridge**	**ICMS**		**Garnet-Orthoamphibole Gneiss**													
TBR83g1sp1	1999-08-18Aug	80	P/A	Matrix	X	2414	8	2295	14	2408	20	2411	10	6.93	99.8	99.14	99.86
TBR83g1sp2	1999-08-18Aug					1924	12	1818	9	1900	13	1912	9	6.73	99.88	98.81	99.85
TBR83g1sp3	1999-08-18Aug					2154	6	1839	8	1957	10	2055	6	6.64	99.9	99.4	99.91
TBR83g1sp4	1999-08-18Aug					2294	10	1999	14	2197	25	2248	12	7.57	99.9	99.41	99.91
TBR83g1sp5	1999-08-18Aug					1987	8	1933	11	1982	12	1985	6	6.18	99.81	98.57	99.81
TBR83g1sp6	1999-08-18Aug					1765	13	1756	17	1881	27	1826	14	5.77	99.75	97.05	99.66
TBR-83a_gr1_sp1	98_08_27Aug\			same as grain 1		1879	4	1788	14					3.68			
TBR-83a_gr1_sp2	98_08_27Aug\					1978	7	1737	50					2.93			
TBR-83a_gr1_sp3	98_08_27Aug\					2226	7	1832	114					2.34			
TBR-83a_gr1_sp4	98_08_27Aug\					2031	6	1850	31					3.28			
TBR83g3sp1	1999-08-18Aug	25	E	Matrix	X	2084	10	1888	13	2015	16	2050	8	5.85	99.92	99.34	99.91
TBR83g3sp2	1999-08-18Aug					2219	11	1899	8	2027	13	2124	8	6.52	99.96	99.7	99.96
TBR83g3sp3	1999-08-18Aug					2327	16	2267	21	2284	28	2307	14	5.32	99.84	98.62	99.78
TBR-83a_gr2_sp1	98_08_27Aug\	50	E	in Cordierite	X	1722	17	1744	64					2.77			
TBR-83a_gr2_sp2	98_08_27Aug\					1948	7	1823	37					3.17			
JDF-13	**Mill Creek**	**ICMS**		**Aluminous Gneiss**													
JDF13_g1	1999-08-21Aug	15	E	in Garnet	X	2474	5	2578	27	2735	29	2587	12	3.39	99.64	94.7	99.23
JDF13_g2	1999-08-21Aug	50	E	Matrix	X	2485	24	2331	49	2458	61	2473	28	4.12	99.98	99.11	99.85
JDF13_g2@1	1999-08-21Aug					2471	20	2433	38	2545	66	2504	29	4.52	99.97	98.67	99.77
JDF13_g2@2	1999-08-21Aug					2455	15	2622	93	2914	116	2651	47	3.34	99.97	99.07	99.84
JDF13_g2@3	1999-08-21Aug					2427	7	2447	15	2600	21	2504	10	5.07	99.6	98.59	99.76
						2451	**22**										
JDF13_g4	1999-08-21Aug	50	E/A	Matrix	X	2068	74	2327	90	2582	122	2305	73	5.45	99.97	99.7	99.95
JDF13_g5	1999-08-21Aug	25	E/A	Matrix	X	2407	6	2414	19	2601	24	2494	10	5.72	99.97	99.46	99.91
TBR-240	**Bivens Creek ridge**	**ICMS**		**Aluminous Gneiss**													
TBR240_gc1	1999-08-21Aug	150	P/A	Matrix	X	2270	9	2170	10	2260	13	2265	7	6.36	99.96	99.77	99.96
TBR240_gc1@1	1999-08-21Aug					1770	8	1713	7	1793	13	1783	8	7.10	99.93	99.43	99.94
TBR240_gc1@2	1999-08-21Aug					1759	6	1685	8	1746	10	1752	6	7.47	99.96	99.63	99.96
TBR240_gc1@3	1999-08-21Aug					1955	9	1844	10	1955	11	1955	7	6.66	99.92	99.43	99.93
TBR240_gc3	1999-08-21Aug	100	P	Matrix	X	2439	5	2450	11	2497	15	2465	7	6.47	99.97	99.76	99.96
TBR240_gc3@1	1999-08-21Aug	50	P	in Quartz	X	1977	5	1858	10	1892	13	1933	7	5.96	99.94	99.63	99.95
TBR-180	**Quartz Creek ridge**	**ICMS**		**Aluminous Gneiss**													
TBR180AgA1	1999-08-22Aug	200	P/A	Matrix	X	1771	7	1601	12	1970	15	1875	8	5.65	99.94	99.26	99.92
TBR180AgA1@1	1999-08-22Aug					1745	9	1565	12	1742	16	1743	9	5.64	99.89	97.43	99.7
TBR180AgA2	1999-08-22Aug	100		Matrix		1760	9	1565	9	1821	14	1792	8	6.10	99.93	99.28	99.92
TBR180AgA2@1	1999-08-22Aug					1740	7	1609	12	1784	16	1764	9	5.72	99.96	99.26	99.92
TBR180AgA2@2	1999-08-22Aug					1753	9	1560	11	1771	15	1763	9	6.05	99.8	96.7	99.62
TBR180AgB3	1999-08-22Aug	30	E/A	in Garnet	X	2576	11	2475	15	2335	17	2466	8	6.63	99.73	98.38	99.7
TBR180AgB3@1	1999-08-22Aug					2459	6	2339	14	2423	20	2443	9	5.97	99.85	99.22	99.87

Sample/Grain/Spot#	Date	Grain Size	Grain	Textural	Xray-map	Age (Ma)	1 s.e.	Age (Ma)	1 s.e.	Age (Ma)	1 s.e.	Age (Ma)	1 s.e.	Th O2/	diogenic	diogenic	diogenic
		microns	Shape*	Setting	X=Map	207Pb/	207Pb/	208Pb/	208Pb/	206Pb/	206Pb/	207Pb/	207Pb/	Th	208Pb	207Pb	206Pb
						206Pb	206Pb	232Th	232Th	238U	238U	235U	235U				
						**	***		***		***		***				
TBR-227d	**Skikhi Ridge**	**ICMS**		**Aluminous Gneiss**													
TBR227d_g1sp1	1999-12-07Dec	500	P	Matrix	X	2464	8	2247	45	2388	32	2429	15	4.741	99.97	99.65	99.94
TBR227d_g1sp2	1999-12-07Dec					2445	13	2127	46	2245	44	2351	20	4.712	99.96	99.47	99.91
TBR227d_g1sp3	1999-12-07Dec					2444	10	2191	43	2322	35	2387	17	4.884	99.97	99.07	99.84
TBR227d_g1sp4	1999-12-07Dec					2381	10	2034	40	2180	31	2286	15	4.815	99.97	99.55	99.93
TBR227d_g1sp5	1999-12-07Dec					2447	12	2173	35	2321	36	2389	16	4.963	99.97	99.27	99.88
TBR227d_g1sp6	1999-12-08Dec					2451	6	2242	15	2399	21	2427	10	4.645	99.97	99.61	99.93
TBR227d_g1sp7	1999-12-08Dec					2463	9	2165	19	2301	19	2388	9	4.862	99.97	99.52	99.92
TBR227d_g1sp8	1999-12-08Dec					2444	12	2199	23	2302	30	2378	13	4.922	99.98	99.37	99.89
TBR227d_g1sp9	1999-12-08Dec					2445	10	2214	19	2320	17	2387	8	4.855	99.97	99.55	99.92
TBR227d_g1sp10	1999-12-08Dec					2410	10	2077	15	2239	20	2330	9	4.723	99.95	99.37	99.9
						2439	**25**										
TBR-227a	**Skikhi Ridge**	**ICMS**		**Aluminous Gneiss**													
TBR227a_g1sp1	1999-12-08Dec	150	E	Matrix	X	2453	7	2089	11	2186	19	2327	9	4.85	99.96	99.39	99.9
TBR227a_g1sp2	1999-12-08Dec					2432	11	2115	18	2280	29	2361	14	4.593	99.96	99.29	99.88
TBR227a_g1sp3	1999-12-08Dec					2457	11	2137	18	2300	30	2384	14	4.598	99.98	99.61	99.93
TBR227a_g1sp4	1999-12-08Dec					2440	14	2227	28	2307	30	2378	14	5.367	99.96	99.3	99.88
TBR227a_g1sp5	1999-12-08Dec					2454	11	2076	22	2198	23	2334	13	4.612	99.96	99.32	99.89
						2447	**11**										
JBB-27b	**IU Field Camp**	**PMMMS**		**Aluminous Gneiss**													
JBB27b_g1sp1	1999-08-19Aug	250	P	Matrix Biotite	X	1765	4	1717	16	1839	18	1804	10	5.14	99.95	99.72	99.97
JBB27b_g1sp2	1999-08-19Aug					1740	6	1721	6	1802	9	1773	6	6.70	99.98	99.86	99.98
JBB27b_g1sp3	1999-08-19Aug					1724	6	1717	6	1773	10	1751	6	6.56	99.97	99.79	99.98
JBB27b_g1sp4	1999-08-19Aug					1748	3	1692	9	1762	12	1756	6	5.84	99.95	99.71	99.97
JBB27b_g1sp5	1999-08-19Aug					1769	3	1673	9	1778	11	1774	6	5.83	99.97	99.85	99.98
JBB27b_g1sp6	1999-08-19Aug					1783	4	1767	7	1823	9	1804	5	6.51	99.97	99.78	99.97
JBB27b_g1sp7	1999-08-19Aug					1770	5	1666	11	1765	14	1767	7	5.61	99.98	99.87	99.98
JBB-27b	98_08_27Aug\			same as grain 1		1768	5	1733	12					3.79			
JBB27b_g3sp1	1999-08-19Aug	60	P	in Kyanite	X	1778	5	1719	7	1802	10	1791	6	6.59	99.98	99.83	99.98
JBB27b_g3sp2	1999-08-19Aug					1779	5	1746	17	1925	22	1856	11	5.22	99.93	99.48	99.94
JBB27b_g3sp3	1999-08-19Aug					1769	10	1559	19	1638	21	1696	12	5.03	99.98	99.81	99.98
						1775	**6**										
JBB-27b_gr2_sp1@1	98_08_27Aug\	50	E/A	in matirix Quartz		1778	6	1769	30					3.28			
JBB-27b_gr2_sp2	98_08_27Aug\					1769	31	1701	24					3.41			
JBB-27b_gr2_sp3	98_08_27Aug\					1759	5	1725	19					3.51			
JBB-27b_gr2_sp4	98_08_27Aug\					1763	5	1671	14					3.68			
JBB-27b_gr2_sp5	98_08_27Aug\					1766	7	1781	24					3.42			
						1767	**7**										
TBR-208	**IU Field Camp**	**PMMMS**		**Aluminous Gneiss**													
TBR208gAsp1	1999-08-20Aug	150	E	Matrix	X	2509	6	2327	10	2425	20	2471	9	7.22	99.96	99.7	99.95
TBR208gAsp2	1999-08-20Aug					2449	6	2335	12	2373	18	2414	8	7.75	99.97	99.57	99.93
TBR208gAsp3	1999-08-20Aug					2433	6	2248	10	2368	13	2403	7	7.21	99.97	99.58	99.93
TBR208gBsp1	1999-08-20Aug	125	E	Matrix	X	2438	6	2327	10	2474	15	2454	7	6.90	99.96	99.46	99.91
TBR208gBsp2	1999-08-20Aug					1767	17	1671	8	1739	11	1752	10	6.93	99.28	90.97	98.88
TBR208gCsp1	1999-08-20Aug	200	E	Matrix	X	2472	4	2414	12	2545	15	2504	6	6.09	99.96	99.69	99.95
TBR208gCsp2	1999-08-20Aug					1866	6	1853	12	1949	13	1909	7	5.87	99.54	94.68	99.33
TBR208gCsp3	1999-08-20Aug					2417	7	2353	11	2501	15	2455	6	6.45	99.96	99.66	99.94
TBR208gCsp4	1999-08-20Aug					2455	5	2345	12	2474	15	2464	7	6.57	99.95	99.75	99.96
TBR208gCsp5	1999-08-20Aug					2460	5	2397	12	2518	19	2486	8	7.49	99.94	99.66	99.94

Sample/Grain/Spot#	Date	Grain Size	Grain	Textural	Xray-map	Age (Ma)	1 s.e.	Age (Ma)	1 s.e.	Age (Ma)	1 s.e.	Age (Ma)	1 s.e.	Th O2/	diogenic	diogenic	diogenic
		microns	Shape*	Setting	X=Map	207Pb/	207Pb/	208Pb/	208Pb/	206Pb/	206Pb/	207Pb/	207Pb/	Th	208Pb	207Pb	206Pb
						206Pb	206Pb	232Th	232Th	238U	238U	235U	235U				
						**	***		***		***		***				
TBR208gCsp6	1999-08-20Aug					2373	5	2194	10	2364	13	2369	6	6.63	99.95	99.44	99.91
TBR-149	**Boulder Lakes**	**PMMMS**		**Aluminous Gneiss**													
TBR149_gA1	1999-08-21Aug	150	P	Matrix	X	2447	5	2337	12	2320	15	2388	7	6.25	99.96	99.7	99.95
TBR149_gA1@1	1999-08-21Aug					2480	7	2236	13	2289	19	2392	8	6.00	99.94	99.36	99.89
TBR149_gA1@2	1999-08-21Aug					2448	6	2280	18	2396	24	2424	12	5.42	99.96	99.66	99.94
TBR149_gA1@3	1999-08-21Aug					2398	19	2159	28	2264	46	2335	24	4.85	99.51	91.47	98.5
						2443	**34**										
TBR149_gA2	1999-08-21Aug	75	P	Matrix	X	2426	5	2338	13	2530	17	2473	8	5.89	99.95	99.64	99.94
TBR149_gA2@1	1999-08-21Aug					2425	6	2199	13	2406	15	2416	7	5.92	99.97	99.67	99.95
						2426	**1**										
TBR-201	**Lake Shore Peak**	**PMMMS**		**Aluminous Gneiss**													
TBR201ga1	1999-08-22Aug	125	E	in Garnet	X	2449	7	2367	12	2495	19	2470	8	6.25	99.98	99.66	99.94
TBR201ga1@1	1999-08-22Aug					2442	5	2260	14	2458	16	2450	8	6.46	99.97	99.65	99.94
TBR201ga1@2	1999-08-22Aug					2440	7	2271	18	2437	27	2438	13	5.59	99.97	99.59	99.93
TBR201ga1@3	1999-08-22Aug					2473	9	2405	34	2513	38	2491	17	4.60	99.92	99.08	99.84
						2451	**15**										
TBR201gb1	1999-08-22Aug	100	E/A	in Garnet	X	2988	5	2371	17	2653	21	2848	9	5.57	99.89	99.63	99.91
TBR201gb1@1	1999-08-22Aug					2586	18	1951	40	2198	45	2406	22	4.38	99.94	99.85	99.97
TBR201gb2	1999-08-22Aug	150	P/A	on Garnet Edge	X	2309	6	2004	15	2141	20	2228	11	5.55	99.95	98.75	99.8
TBR201gb2@1	1999-08-22Aug					2329	6	1992	18	2187	22	2261	11	5.22	99.97	99.2	99.87
TBR201gb2@2	1999-08-22Aug					2365	8	2094	16	2290	25	2330	11	5.45	99.97	99.19	99.87
TBR201gb2@3	1999-08-22Aug					2432	5	2225	14	2365	17	2401	7	5.69	99.97	99.58	99.93
JBB97-31g	**Cataract Mtn**	**PMMMS**		**Aluminous Gneiss**													
jbb97_31gBsp1	1999-12-08Dec	200	P/A	Matrix	X	2448	9	2024	22	2188	24	2325	13	4.454	99.97	99.78	99.96
jbb97_31gBsp2	1999-12-08Dec					2457	12	2085	23	2203	30	2337	14	4.627	99.97	99.8	99.97
jbb97_31gBsp3	1999-12-08Dec					2447	16	2074	35	2216	50	2338	24	4.698	99.97	99.74	99.96
jbb97_31gBsp4	1999-12-08Dec					2434	12	1981	30	2163	30	2305	15	4.436	99.97	99.76	99.96
jbb97_31gBsp5	1999-12-08Dec					2459	11	1970	23	2080	29	2277	15	4.582	99.97	99.79	99.96
						2449	**10**										
JBB_`97_31g1so1	1999-12-09Dec	100	P/A	Matrix	X	2457	6	2338	13	2351	17	2408	8	5.118	99.97	99.75	99.96
JBB_`97_31g1sp2	1999-12-09Dec					2522	8	2290	14	2332	16	2435	6	5.266	99.95	99.79	99.96
JBB_`97_31g1sp3	1999-12-09Dec					2524	7	2381	18	2413	18	2474	8	5.421	99.94	99.79	99.96
JBB_`97_31g1sp4	1999-12-09Dec					2463	8	2366	15	2476	19	2469	8	5.103	99.96	99.69	99.95
JBB_`97_31g2sp6	1999-12-09Dec					2454	7	2087	37	2098	34	2284	17	4.192	99.97	99.79	99.96
TBR-129	**Leggatt Ridge**	**SPMS**		**Aluminous Gneiss**													
TBR129g2s1	1999-08-16Aug	75	E/A	in Biotite	X	1746	61	1696	124	1879	154	1817	83				
TBR129_g2s6	1999-08-17Aug					1738	38	1421	41	1533	59	1621	34	4.73	99.98	98.76	99.86
TBR129_g2s7	1999-08-17Aug					1920	31	1588	60	1680	89	1790	53	3.65	99.96	97.14	99.64
TBR129_g2s8	1999-08-17Aug					1713	18	1437	25	1510	33	1597	22	6.79	99.94	99.55	99.95
TBR129_g2s9	1999-08-17Aug					1738	19	1553	18	1683	29	1708	16	6.48	99.69	97.51	99.71
TBR129_g2s10	1999-08-17Aug					1716	18	1491	32	1563	40	1629	21	5.72	99.98	99.7	99.97
TBR129_g2s11	1999-08-17Aug					1756	43	1598	67	1896	99	1830	52	3.36	99.96	97.66	99.73
TBR129_g2s12	1999-08-17Aug					1740	25	1586	41	1718	63	1728	35	4.86	99.98	98.48	99.83
TBR-129_Mon2_sp1	98_08_28aug \			same as grain 2		1753	3	1606	7					4.35			
TBR129_g8s2	1999-08-17Aug	60	E	in Cordierite	X	1765	27	1680	38	1624	73	1686	43	6.32	99.92	98.54	99.83

Sample/Grain/Spot#	Date	Grain Size	Grain	Textural	Xray-map	Age (Ma)	1 s.e.	Age (Ma)	1 s.e.	Age (Ma)	1 s.e.	Age (Ma)	1 s.e.	Th O2/	diogenic	diogenic	diogenic
		microns	Shape*	Setting	X=Map	207Pb/	207Pb/	208Pb/	208Pb/	206Pb/	206Pb/	207Pb/	207Pb/	Th	208Pb	207Pb	206Pb
						206Pb	206Pb	232Th	232Th	238U	238U	235U	235U				
						**	***		***		***		***				
TBR129_g9s1	1999-08-17Aug	110	P/A	Crd-Grt-Sill mass	X	1713	19	1593	21	1618	30	1659	20	6.61	99.95	99.7	99.97
TBR129_g9s2	1999-08-17Aug					1763	16	1681	16	1837	28	1802	14	6.57	99.94	98.91	99.88
TBR129_g9s3	1999-08-17Aug					1747	20	1584	23	1580	29	1653	20	6.98	99.91	99.15	99.9
TBR129_g9s4	1999-08-17Aug					1753	6	1680	10	1703	14	1726	8	6.20	99.95	99.68	99.96
TBR129_g9s5	1999-08-17Aug					1776	9	1652	10	1652	14	1708	8	6.57	99.92	99.45	99.94
TBR129_g9s7	1999-08-17Aug					1771	7	1623	12	1691	15	1727	8	5.72	99.97	99.72	99.97
TBR129_g9s8	1999-08-17Aug					1767	11	1561	8	1741	16	1753	10	6.75	99.86	98.58	99.84
TBR-129_Mon1_sp1	98_08_28aug \		P/A	same as grain 9		1747	13	1671	41					3.35			
TBR-129_Mon3_sp1	98_08_28aug \	85	P/A	Mztrix		1772	9	1593	8					4.19			
TBR-129_Mon3_sp2	98_08_28aug \					1765	4	1496	9					3.76			
TBR-16	**Nobel Lake Ridge**	**SPMS**		**Garnet-Orthoamphibole Gneiss**													
TBR16_g1sp1	1999-08-18Aug	100	E/A	Matrix	X	1740	9	1676	8	1709	15	1723	8	6.86	99.92	98.78	99.86
TBR16_g1sp2	1999-08-18Aug					1785	9	1660	9	1756	14	1769	8	7.16	99.96	99.45	99.94
TBR16_g1sp3	1999-08-18Aug					1756	9	1669	9	1738	13	1746	8	7.22	99.96	99.33	99.92
TBR16_g1sp4	1999-08-18Aug					1764	9	10	0	1806	18	1787	10	7.09	92.54	98.7	99.85
TBR-16_gr1_sp1	98_08_27Aug\			same as gr 1		1748	6	1528	9					3.64			
TBR-16_gr1_sp2	98_08_27Aug\					1772	5	1626	9.99					3.62			
TBR-16_gr1_sp3	98_08_27Aug\					1749	7	1656	18					3.54			
						1759	**16**										
TBR16_g2sp1	1999-08-18Aug	100	P/A	Matrix	X	1771	9		0	1909	14	1844	9	6.48	91.24	99.06	99.89
TBR16_g2sp2	1999-08-18Aug					1758	11	1650	13	1739	23	1748	13	5.50	99.98	99.24	99.91
TBR-16_gr2_sp1	98_08_27Aug\			same as gr 2		1751	7	1601	10					3.89			
TBR-16_gr2_sp2	98_08_27Aug\					1756	26	1662	15					3.77			
						1759	**9**										
TBR16_g3sp2	1999-08-18Aug	100	E/A	Matrix	X	1757	13	1678	7	1738	17	1746	10	7.04	99.95	98.49	99.83
TBR16_g3sp3	1999-08-18Aug					1759	11	1687	7	1733	16	1744	10	7.23	99.94	98.25	99.8
TBR16g3	1999-08-18Aug					1738	21	1680	47	1722	65	1729	35	7.33	99.82	95.34	99.45
TAH-18i	**Sunrise Lake**	SPMS		**Aluminous Gneiss**													
TAH18i_g1sp1	1999-08-19Aug	120	P/A	in matrix/ Garnet Rim	X	1715	15	1629	7	1659	16	1684	10	7.20	99.95	92.05	99.05
TAH18i_g1sp2	1999-08-19Aug					1734	37	1377	24	1595	31	1656	22	5.34	99.91	90.75	98.87
TAH18i_g1sp3	1999-08-19Aug					1730	13	1641	9	1744	20	1738	13	6.19	99.96	93.27	99.2
TAH18i_g1sp4	1999-08-19Aug					1752	9	1723	7	1793	15	1774	8	7.49	99.97	98.11	99.78
TAH-18i_gra_sp1	98_08_27Aug\			**??same as gr 1**		1775	5	1655	13					3.95			
TAH-18i_gra_sp2	98_08_27Aug\			looks like gr 6		1774	7	1725	17					3.58			
TAH-18i_gra_sp2@1	98_08_27Aug\					1771	11	1767	16					3.67			
TAH18i_g2sp2	1999-08-19Aug	50	E/A	Matrix	X	1752	15	1699	8	1821	19	1789	12	6.46	99.94	94.86	99.39
TAH18i_g6sp2	1999-08-19Aug					1742	5	1694	8	1820	9	1784	5	6.30	99.94	99.21	99.91
TAH-18i_gr2_sp1	98_08_27Aug\			same as gr 2		1585	148	1777	16					4.16			
TAH-18i_gr2_sp2	98_08_27Aug\					1728	21	1803	12					3.91			
TAH-18i_gr2_sp3	98_08_27Aug\					1727	20	1666	13					3.79			
TAH-18i_gr3_sp1	98_08_27Aug\	50	E/A	in matrix w/ Ky	X	1720	24	1623	15					3.64			
TAH-18i_gr3_sp2	98_08_27Aug\					1740	57	1738	17					3.94			
TAH-18i_gr3_sp3	98_08_27Aug\					1739	43	1641	24					3.46			
TAH-18i_gr4_sp1	98_08_27Aug\	70	P/A	in Kyanite		1753	8	1709	14					3.69			
TAH-18i_gr4_sp2	98_08_27Aug\					1760	13	1462	13					3.69			
TAH18i_g6sp1	1999-08-19Aug	50	E/A	in Garnet		1771	8	1738	8	1828	17	1801	8	6.63	99.93	99.16	99.9

Sample/Grain/Spot#	Date	Grain Size	Grain	Textural	Xray-map	Age (Ma)	1 s.e.	Age (Ma)	1 s.e.	Age (Ma)	1 s.e.	Age (Ma)	1 s.e.	Th O2/	diogenic	diogenic	diogenic
		microns	Shape*	Setting	X=Map	207Pb/	207Pb/	208Pb/	208Pb/	206Pb/	206Pb/	207Pb/	207Pb/	Th	208Pb	207Pb	206Pb
						206Pb	206Pb	232Th	232Th	238U	238U	235U	235U				
						**	***		***		***		***				
TBR-251a	**Thompson Peak Ridg**	**SPMS**		**Aluminous Gneiss**													
TBR251a_g1sp1	1999-08-19Aug	60	E/A	Matrix	X	1786	6	1765	7	1873	10	1832	5	6.44	99.99	99.89	99.99
TBR251a_g1sp2	1999-08-19Aug					1772	5	1721	7	1779	10	1776	6	6.68	99.98	99.77	99.97
TBR251a_g1sp3	1999-08-19Aug					1761	5	1697	8	1776	9	1769	5	6.14	99.98	99.78	99.98
TBR251a_g1sp4	1999-08-19Aug					1773	20	1524	22	1617	23	1686	13	5.74	99.97	99.8	99.98
TBR251a_g1sp5	1999-08-19Aug					1773	4	1669	16	1740	17	1755	9	5.26	99.99	99.87	99.99
						1773	**9**										
TBR-110A	**Nobel Lale**	**SPMS**		**Aluminous Gneiss**													
TBR110AgBsp1	1999-08-20Aug	75	E	Matrix		1782	9	1651	10	1773	12	1777	7	7.25	99.93	99.32	99.92
TBR110AgBsp2	1999-08-20Aug					1768	11	1634	9	1573	15	1658	10	6.98	99.88	98.38	99.81
TBR110AgBsp3	1999-08-20Aug					1757	11	1690	8	1651	18	1698	10	6.65	99.83	97.98	99.77
						1769	**13**										
TBR-110B	**Nobel Lake**	**SPMS**		**Aluminous Gneiss**													
TBR110BgB1	1999-08-22Aug	250	P	Matrix		1757	7	1775	12	1840	16	1801	8	5.71	99.93	99.64	99.96
TBR110BgB1@1	1999-08-22Aug					1721	6	1782	14	1846	15	1788	9	5.55	99.84	99.14	99.9
TBR110BgB1@3	1999-08-22Aug					1769	6	1753	8	1828	9	1800	5	6.25	99.96	99.69	99.96
TBR110BgB2	1999-08-22Aug	30	E	Matrix	X	1838	8	1809	13	1813	17	1824	10	5.56	99.93	99.49	99.94
TBR110BgB2@1	1999-08-22Aug					1755	7	1778	12	1861	16	1811	8	5.77	99.92	99.56	99.95
TBR-189	**Nobel Lale**	**SPMS**		**Aluminous Gneiss**													
TBR189gAsp1	1999-08-20Aug	100	E/A	Matrix		1783	5	1693	11	1749	12	1765	6	5.81	99.94	99.49	99.94
TBR189gAsp2	1999-08-20Aug					1781	7	1690	7	1697	9	1735	6	7.04	99.88	99.51	99.94
						1782	**1**										
TBR189gbsp1	1999-08-20Aug	50	E	Matrix		1781	6	1745	11	1686	11	1729	6	6.16	99.78	98.89	99.87
TBR189gbsp2	1999-08-20Aug					1765	10	1503	15	1492	16	1609	10	5.80	99.85	99.42	99.93
						1773	**11**										
TBR189gCsp1	1999-08-20Aug	60	E	Matrix		1749	14	1692	8	1680	20	1711	11	6.84	99.94	96.59	99.6
TBR189gCsp2	1999-08-20Aug					1730	15	1677	10	1688	20	1707	11	6.10	99.97	97.98	99.77
						1740	**13**										
TBR-138	**Leggatt Ridge**	**SPMS**		**Garnet-Orthoamphibole Gneiss**													
TBR138_g1	1999-08-21Aug	50	E	Matrix		1777	13	1687	8	1726	20	1749	12	6.99	99.89	97.64	99.72
TBR138g5sp1@1	1999-08-21Aug	50	E/A	Matrix		1785	12	1696	12	1654	26	1712	15	7.37	99.81	99.02	99.89
TBR138_g7sp1	1999-08-21Aug	100	E	Matrix		1771	8	1644	8	1646	11	1702	7	7.06	99.91	99.43	99.93
TBR138_g7sp1@1	1999-08-21Aug			Matrix		1774	11	1644	19	1723	24	1746	12	6.09	98.56	97.97	99.76
TBR138_g8	1999-08-21Aug	50	P	in Cord after Gar		1776	12	1689	11	1736	15	1754	10	5.97	99.51	97.32	99.68
						1777	**5**										
TBR-54	**Granite Peak ridge**	**SPMS**		**Garnet-Orthoamphibole Gneiss**													
TBR54gai	1999-08-22Aug	150	E	Matrix	X	1866	9	1696	13	1556	16	1692	9	7.01	99.96	99.55	99.95
TBR54gai@1	1999-08-22Aug					1785	11	1633	8	1722	17	1750	7	6.55	99.95	99.57	99.95
TBR54gai@2	1999-08-22Aug					1741	13	1486	11	1602	20	1663	10	7.04	99.96	98.64	99.85
TBR54gai@3	1999-08-22Aug					1749	31	1647	22	1739	32	1744	15	6.90	99.91	96.56	99.6
						1785	**57**										

Sample/Grain/Spot#	Date	Grain Size	Grain	Textural	Xray-map	Age (Ma)	1 s.e.	Age (Ma)	1 s.e.	Age (Ma)	1 s.e.	Age (Ma)	1 s.e.	Th O2/	diogenic	diogenic	diogenic
		microns	Shape*	Setting	X=Map	207Pb/	207Pb/	208Pb/	208Pb/	206Pb/	206Pb/	207Pb/	207Pb/	Th	208Pb	207Pb	206Pb
						206Pb	206Pb	232Th	232Th	238U	238U	235U	235U				
						**	***		***		***		***				
TBR-10	**Thopmson Peak Ridg**	**SPMS**		**Garnet-Orthoamphibole Gneiss**													
TBR10_4s1g1	1999-12-06Dec	175	P	in Cord after Garnet		1786	7	1698	14	1776	17	1781	10	4.80	99.95	99.60	99.95
TBR10_4g1sp2	1999-12-06Dec					1795	7	1701	13	1711	19	1749	11	4.98	99.94	99.42	99.93
TBR10_4g1sp3	1999-12-06Dec					1823	9	1604	9	1578	12	1686	8	5.29	99.97	99.40	99.93
TBR10_4gr1sp4	1999-12-06Dec					1753	11	1603	15	1732	23	1741	14	4.73	99.96	98.96	99.88
TBR10_4gr1sp5	1999-12-06Dec					1748	10	1619	20	1793	26	1772	14	4.50	99.97	99.16	99.90
TBR10_4gr1sp6	1999-12-06Dec					1770	7	1662	9	1560	10	1651	5	5.32	99.96	99.68	99.96
TBR10_4gr1sp7	1999-12-06Dec					1765	8	1598	16	1602	22	1674	13	4.69	99.95	99.29	99.92
TBR10_4gr1sp8	1999-12-06Dec					1768	7	1552	15	1596	16	1671	10	4.74	99.95	99.27	99.92
TBR10_4gr1sp8	1999-12-06Dec					1769	8	1555	13	1596	18	1672	11	5.06	99.97	99.40	99.93
TBR10_4gr1sp10	1999-12-06Dec					1767	7	1597	21	1632	23	1692	13	4.56	99.97	99.27	99.92
TBR10_gr2bsp1	1999-12-06Dec	110	E	in Cord after Garnet		1762	12	1492	9	1533	17	1632	10	5.52	99.96	99.65	99.96
TBR10_gr2bsp2	1999-12-06Dec					1768	10	1502	9	1575	10	1659	6	5.54	99.97	99.70	99.97
TBR10_gr2bsp3	1999-12-06Dec					1771	9	1593	10	1559	13	1652	8	5.87	99.96	99.63	99.96
TBR10_gr2bsp4	1999-12-06Dec					1772	9	1605	16	1837	19	1807	10	4.91	99.95	99.72	99.97
TBR10_gr2bsp5	1999-12-06Dec					1766	10	1403	21	1713	26	1737	14	4.95	99.97	99.40	99.93
TBR10_gr2bsp6	1999-12-06Dec					1763	9	1369	16	1622	22	1685	12	4.73	99.97	99.58	99.95
						1767	**4**										
KAT-20	**Thopmson Peak Ridg**	**SPMS**		**Garnet-Orthoamphibole Gneiss**													
KAT20_g1sp1	1999-12-07Dec	150	E/A	Matrix		1765	9	1510	19	1594	21	1669	11	5.19	99.81	98.07	99.78
KAT20_g1sp2	1999-12-07Dec					1770	10	1581	26	1695	29	1729	17	5.11	99.89	99.00	99.89
KAT20_g1sp3	1999-12-07Dec					1770	9	1320	27	1452	21	1587	13	4.78	99.91	99.31	99.92
KAT20_g1sp4	1999-12-07Dec					1760	12	1505	11	1521	13	1624	8	5.63	99.74	97.79	99.74
						1766	**5**										
KAT20_g2sp1	1999-12-07Dec	100	E/A	Matrix		1773	7	1576	22	1659	19	1710	11	5.03	99.97	99.61	99.96
KAT20_g2sp2	1999-12-07Dec					1764	9	1534	30	1632	26	1691	14	4.79	99.97	99.61	99.96
KAT20_g2sp3	1999-12-07Dec					1720	8	1602	12	1614	15	1660	9	5.43	99.85	99.58	99.95
KAT20_g2sp4	1999-12-07Dec					1734	9	1572	24	1704	21	1717	12	4.96	99.77	97.80	99.75
TBR-6	**Thopmson Peak Ridg**	SPMS		**Garnet-Orthoamphibole Gneiss**													
TBR6_g1sp1	1999-12-07Dec	125	P	in Biotite		1765	10	1557	14	1643	17	1697	10	5.31	99.96	99.25	99.91
TBR6_g1sp2	1999-12-07Dec					1766	10	1508	10	1589	19	1667	11	5.45	99.97	99.00	99.89
TBR6_g1sp3	1999-12-07Dec					1764	15	1483	10	1522	21	1626	13	5.51	99.97	99.01	99.89
						1765	**1**										
TBR6_g2sp1	1999-12-07Dec	100	E	in Biotite		1774	10	1624	10	1719	13	1744	7	5.48	99.92	99.45	99.94
TBR6_g2sp2	1999-12-07Dec					1750	13	1631	19	1665	30	1702	17	5.65	99.96	98.98	99.88
TBR6_g2sp3	1999-12-07Dec					1759	12	1498	13	1577	17	1656	10	5.30	99.96	99.14	99.90
						1761	**12**										
TBR6_g3sp1	1999-12-07Dec	50	E	in Biotite		1774	12	1605	17	1690	18	1728	12	5.34	99.94	99.08	99.89
TBR6_g3sp12	1999-12-07Dec					1748	13	1548	15	1650	22	1693	12	5.28	99.96	99.17	99.91
JBB95-36a	**Rossitter Lake**	SPMS		**Aluminous Gneiss**													
JBB95_36a_g1Bsp1	1999-12-08Dec	50	E/A	in Ilm in sill		1752	14	1678	18	1560	21	1644	13	6.436	99.67	95.45	99.46
JBB95_36a_g1Bsp2	1999-12-08Dec					1761	13	1698	15	1780	24	1771	13	5.159	99.93	99.05	99.89
JBB95_36a_g1Bsp3	1999-12-08Dec					1776	16	1623	16	1634	23	1697	11	4.994	99.9	**98.5**	99.83
						1763	**12**										

Sample/Grain/Spot#	Date	Grain Size	Grain	Textural	Xray-map	Age (Ma)	1 s.e.	Age (Ma)	1 s.e.	Age (Ma)	1 s.e.	Age (Ma)	1 s.e.	Th O2/	diogenic	diogenic	diogenic
		microns	Shape*	Setting	X=Map	207Pb/	207Pb/	208Pb/	208Pb/	206Pb/	206Pb/	207Pb/	207Pb/	Th	208Pb	207Pb	206Pb
						206Pb	206Pb	232Th	232Th	238U	238U	235U	235U				
						**	***		***		***		***				
JBB97-14b	**Leggatt Ridge**	**SPMS**		**Aluminous Gneiss**													
JBB97_14b_g1asp1	1999-12-08Dec	300	P	Matrix		1716	29	1492	19	1566	21	1631	16	4.632	99.95	**93.64**	99.25
JBB97_14b_g1asp2	1999-12-08Dec					1736	70	1492	11	1552	32	1632	37	4.708	99.78	**87.23**	98.37
JBB97_14b_g1asp3	1999-12-08Dec					1669	115	1082	13	1350	27	1479	53	4.24	99.45	**59.54**	93.12
JBB97_14b_g1asp4	1999-12-08Dec					1773	23	1401	13	1452	33	1588	21	4.513	99.97	**97.11**	99.66
JBB97_14b_g1asp5	1999-12-08Dec					1765	52	1422	11	1484	30	1604	32	4.679	99.79	**87.81**	98.44
JBB97_14b_gMsp1	1999-12-08Dec	125	E/A	Matrix		1726	28	1563	9	1639	37	1678	23	5.423	99.96	94.41	99.34
JBB97_14b_gMsp2	1999-12-08Dec					1713	31	1548	10	1677	31	1693	17	5.574	99.91	89.88	98.77
JBB97_14b_gMsp3	1999-12-08Dec					1737	27	1516	9	1633	48	1679	28	5.046	99.96	94.7	99.38
JBB97_14b_gMsp4	1999-12-08Dec					1717	27	1516	21	1593	36	1647	21	5.381	99.97	95.88	99.52
						1723	**11**										
JBB97-29c	**Cataract Mtn.**	SPMS		**Garnet-Orthoamphibole Gneiss**													
JBB97_29c_g2sp1	1999-12-08Dec	150	E	Matrix		1759	10	1607	12	1606	14	1673	9	5.247	99.96	98.76	99.86
JBB97_29c_g2sp2	1999-12-08Dec					1728	15	1539	10	1540	15	1621	11	5.19	99.91	96.64	99.61
JBB97_29c_g2sp3	1999-12-08Dec					1746	15	1520	9	1528	21	1622	15	5.603	99.89	96.13	99.55
JBB97_29c_g2sp4	1999-12-08Dec					1727	15	1545	11	1532	17	1616	9	5.429	99.94	98.13	99.79
						1740	**15**										
JBB95-39A	**Cataract Mtn.**	**SPMS**		**Quartzofeldspathic Gneiss**													
JBB95_39Ag2sp1	1999-12-09Dec	80	E	Matrix		1717	12	1435	12	1463	14	1570	10	4.804	99.84	95.69	99.5
JBB95_39Ag2sp2	1999-12-09Dec					1737	11	1541	12	1550	12	1631	8	5.06	99.96	98.97	99.88
JBB95_39Ag2sp3	1999-12-09Dec					1739	17	1326	31	1275	30	1459	20	3.948	99.97	99.11	99.9
						1731	**12**										
RBB-3	**Leggatt Saddle**	SPMS		**Quartzite**													
RBB3_g2sp1	1999-12-09Dec	100		Matrix		469	417	79	1	77	1	91	17	4.462	87.98	14.27	73.68
RBB3_g2sp3	1999-12-09Dec		E/A	cluster of 4 grains		0	0	74	1	83	2	46	24	4.436	94.97	8.998	78.5
RBB3_g2sp4	1999-12-09Dec					0	0	76	1	72	2	11	23	4.469	84.45	1.189	61.97
RBB3_g2sp4@1	1999-12-09Dec					1750	52	1420	15	1703	43	1724	34	4.804	98.38	57.11	92.17
*** Grain shape codes: P=prismatic E=Equant A denote irregular or anhedral shape**																	
**** Boxes outline spot ages that are averaged and the average is shown in the boxes outlined by dark lines.**																	
The number to the right of the average, in the dark-lined boxes, is the standard devaition of the average																	
***** These are one sima standard errors**																	

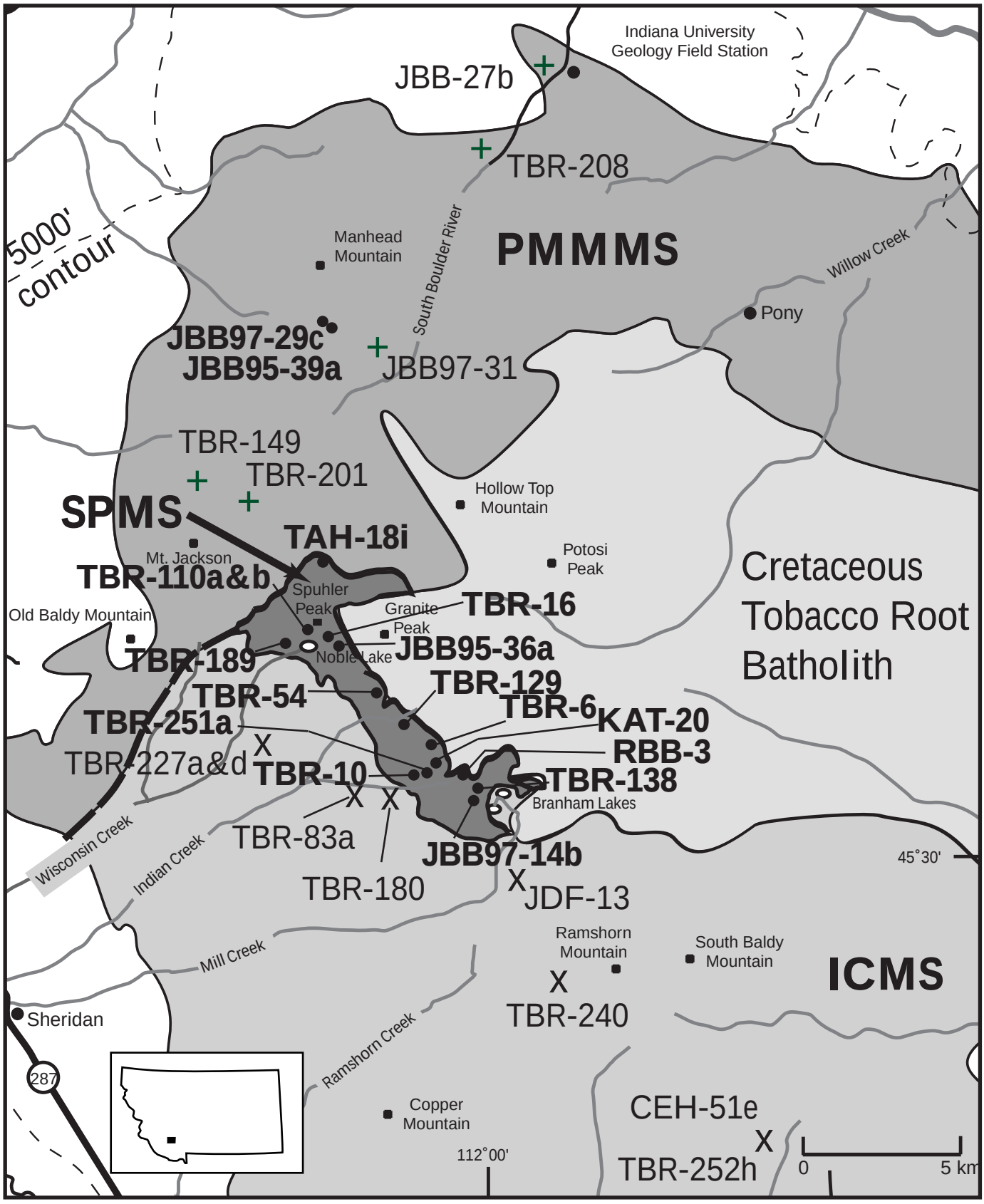
Indiana University
Geology Field Station
JBB-27b
TBR-208
5000'
contour
Manhead
Mountain
South Boulder River
PMMMS
Willow Creek
Pony
JBB97-29c
JBB95-39a
JBB97-31
TBR-149
TBR-201
SPMS
Hollow Top
Mountain
TAH-18i
Mt. Jackson
Potosi
Peak
TBR-110a&b
Spuhler
Peak
Granite
Peak
TBR-16
Cretaceous
Tobacco Root
Batholith
Old Baldy Mountain
Noble Lake
JBB95-36a
TBR-189
TBR-129
TBR-54
TBR-6
KAT-20
TBR-251a
RBB-3
TBR-227a&d
TBR-10
TBR-138
Branham Lakes
Wisconsin Creek
Indian Creek
TBR-83a
JBB97-14b
45°30'
TBR-180
JDF-13
Ramshorn
Mountain
South Baldy
Mountain
ICMS
Mill Creek
TBR-240
Sheridan
Ramshorn Creek
287
Copper
Mountain
CEH-51e
112°00'
TBR-252h
0
5 km

A) SPMS

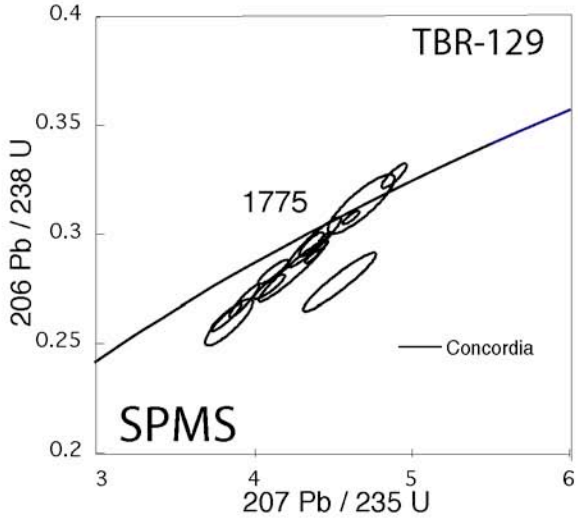

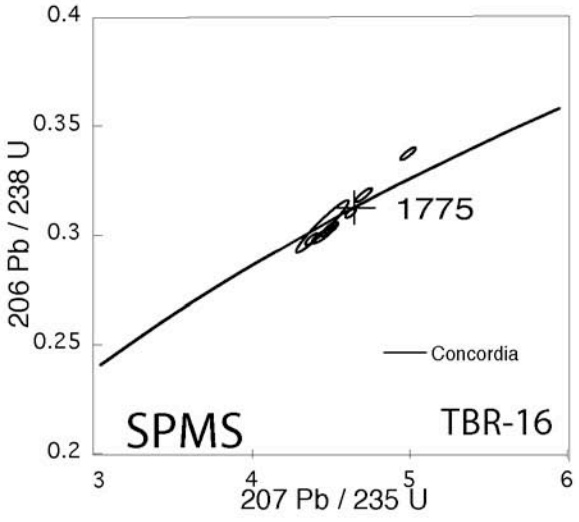

B) ICMS

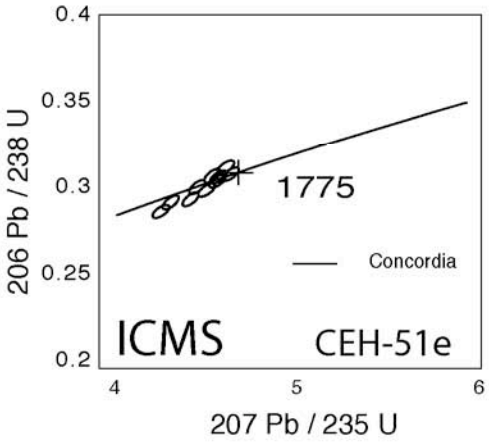

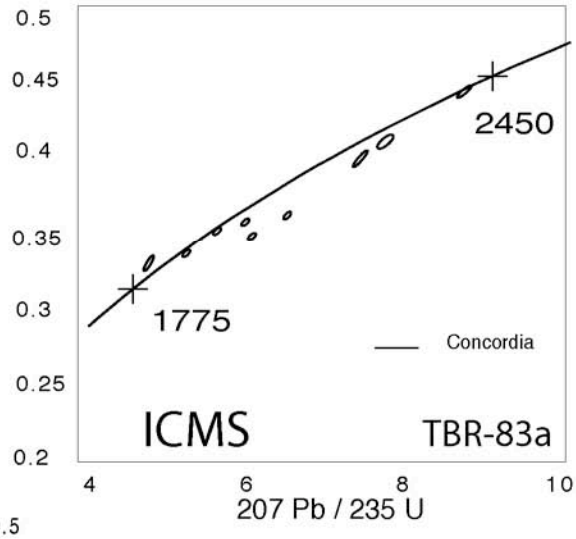

C) PMMMS

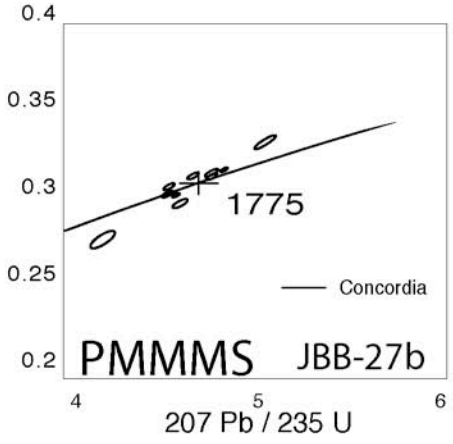

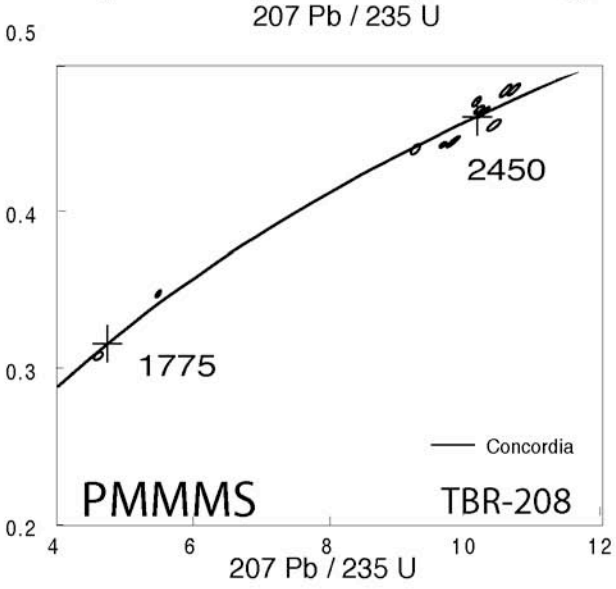

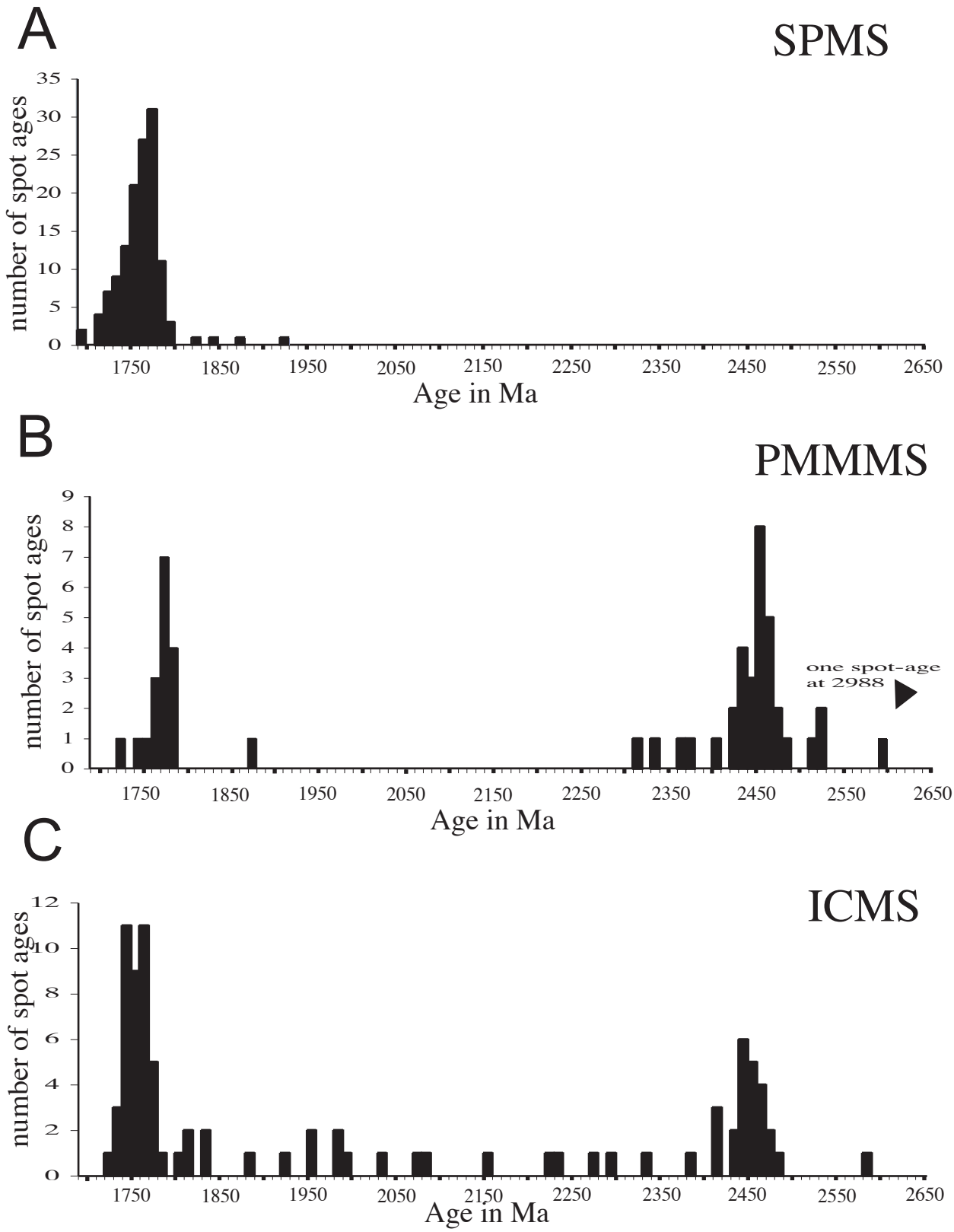
A
SPMS
number of spot ages
0
5
10
15
20
25
30
35
1750
1850
1950
2050
2150
2250
2350
2450
2550
2650
Age in Ma
B
PMMMS
number of spot ages
0
1
2
3
4
5
6
7
8
9
one spot-age
at 2988
1750
1850
1950
2050
2150
2250
2350
2450
2550
2650
Age in Ma
C
ICMS
number of spot ages
0
2
4
6
8
10
12
1750
1850
1950
2050
2150
2250
2350
2450
2550
2650
Age in Ma

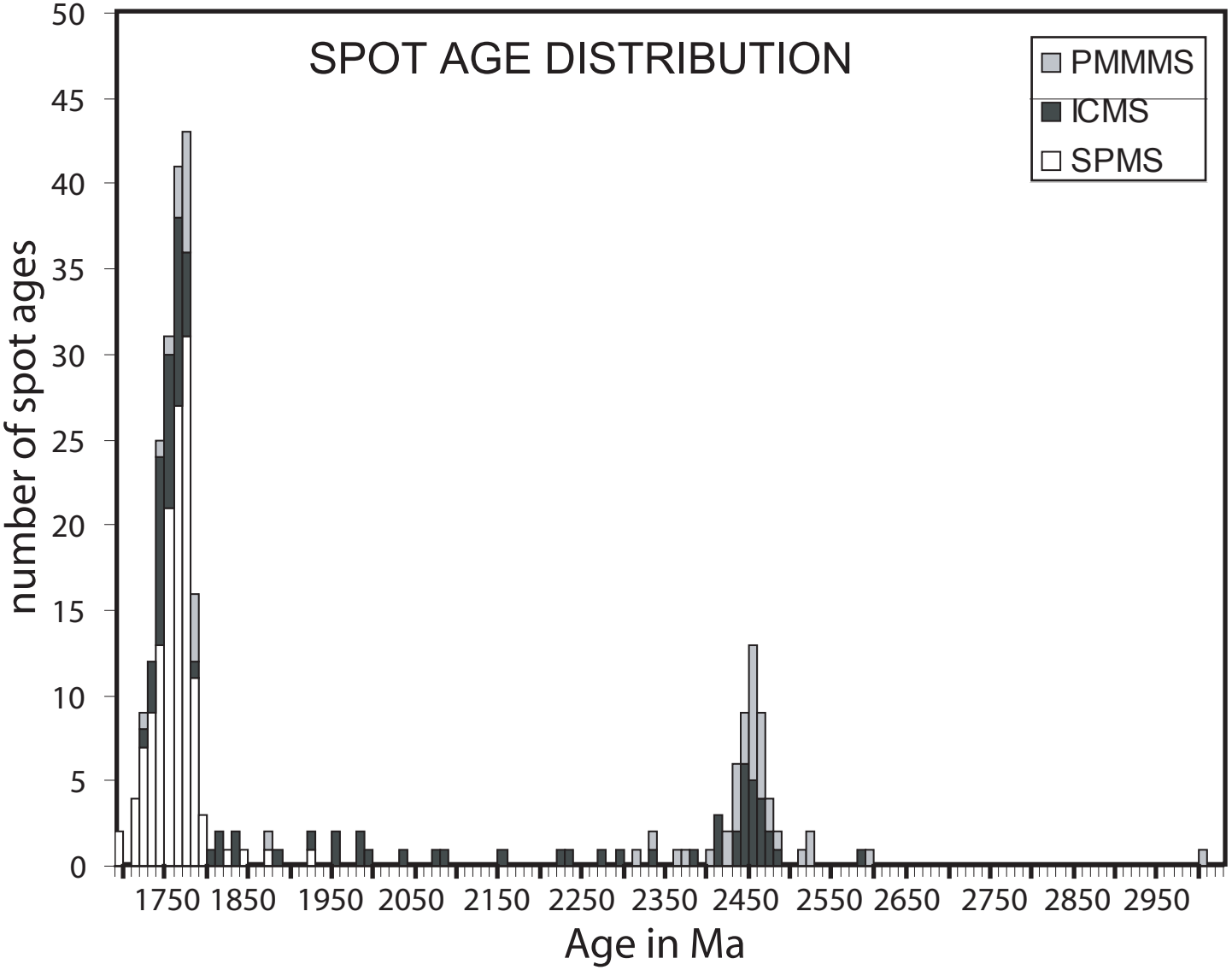
SPOT AGE DISTRIBUTION
PMMMS
ICMS
SPMS
number of spot ages
0
5
10
15
20
25
30
35
40
45
50
1750 1850 1950 2050 2150 2250 2350 2450 2550 2650 2750 2850 2950
Age in Ma

SPMS

TBR-129 GRAIN 9

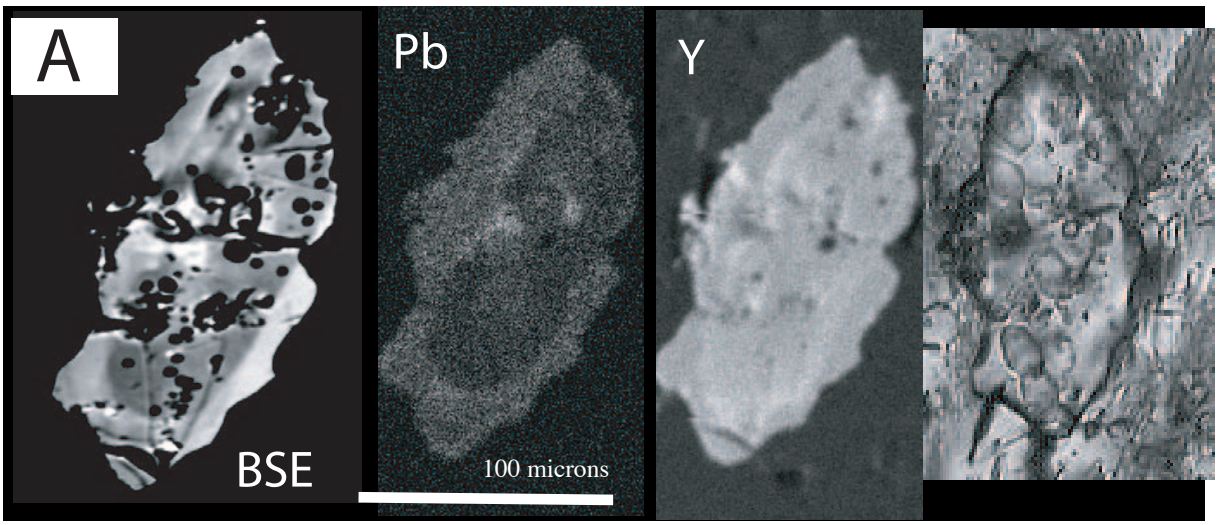

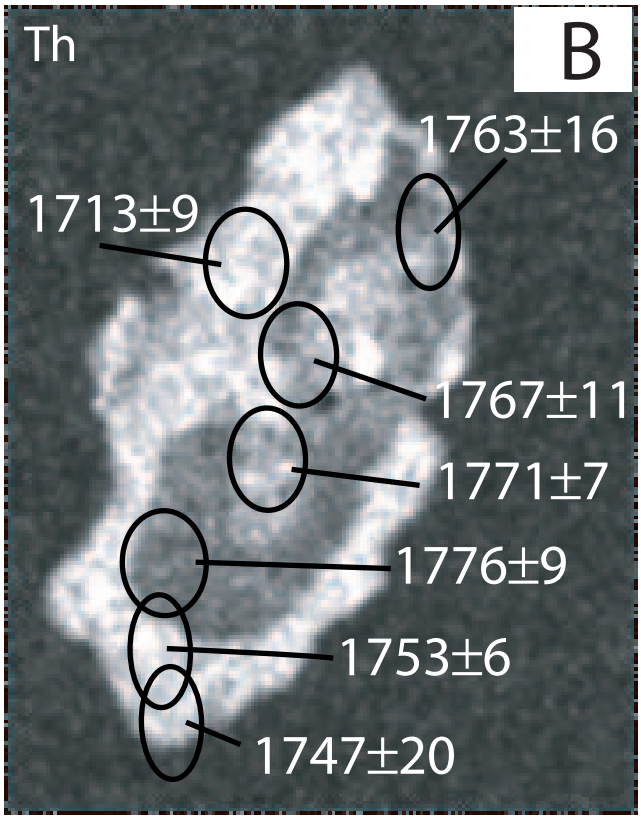

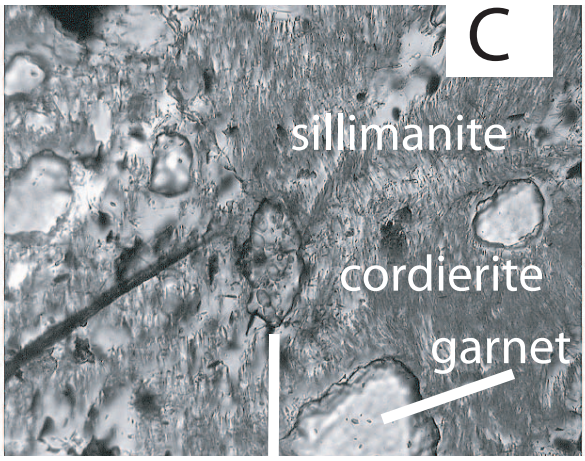

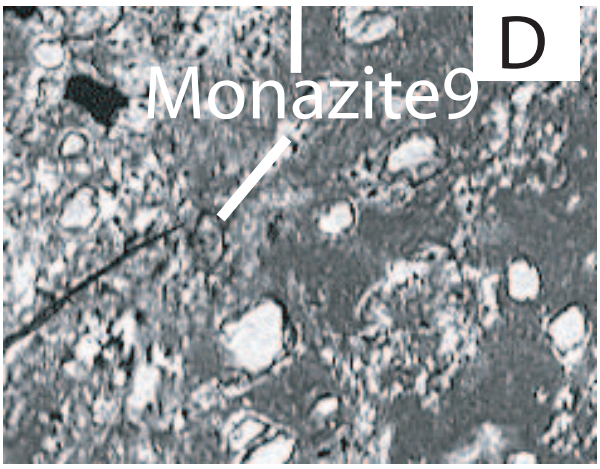

SPMS

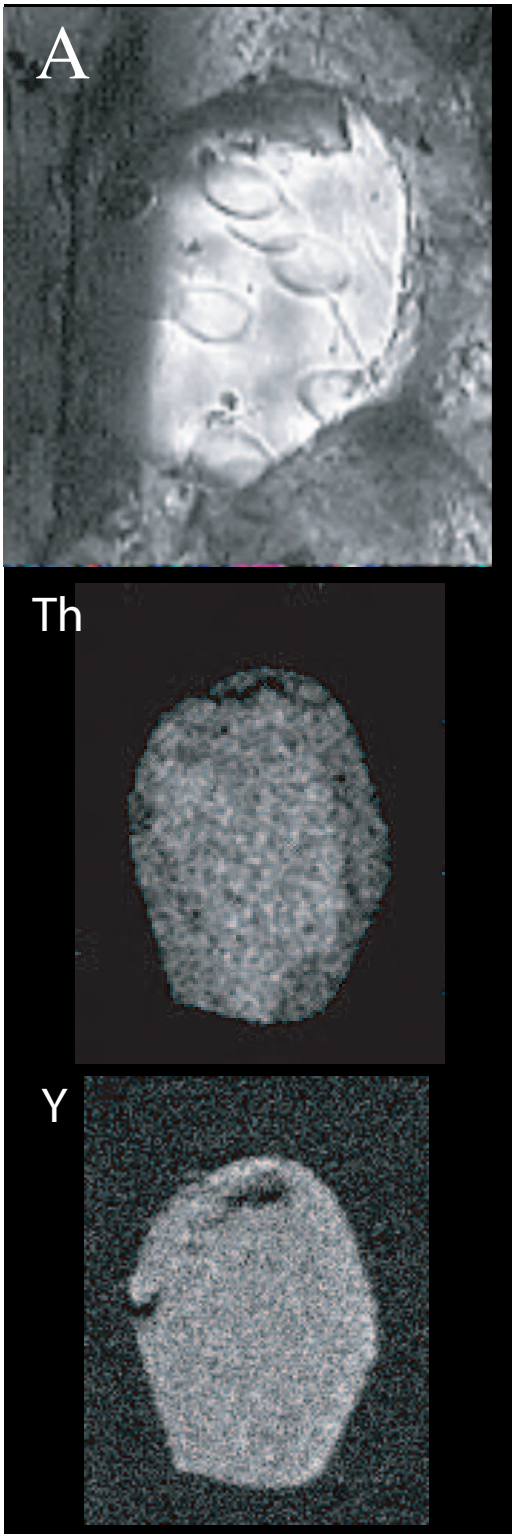

TBR-129 grain 2

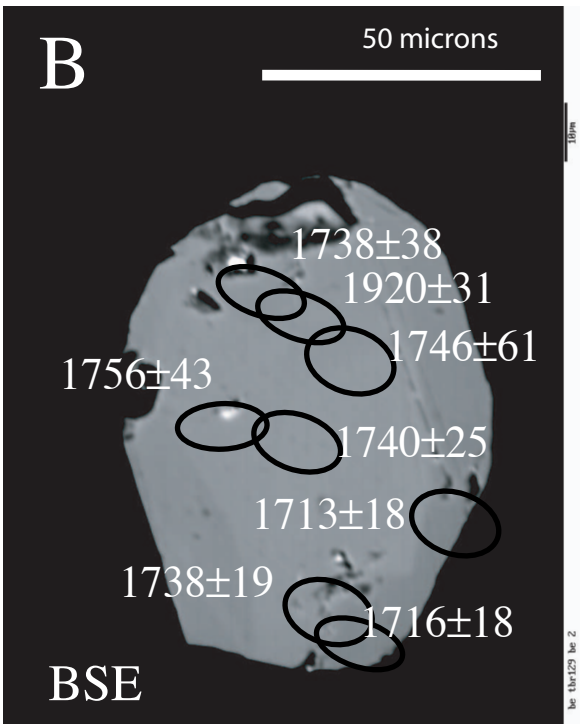

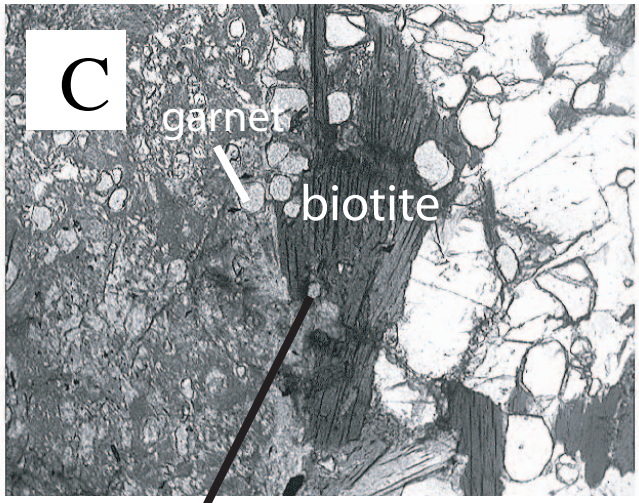

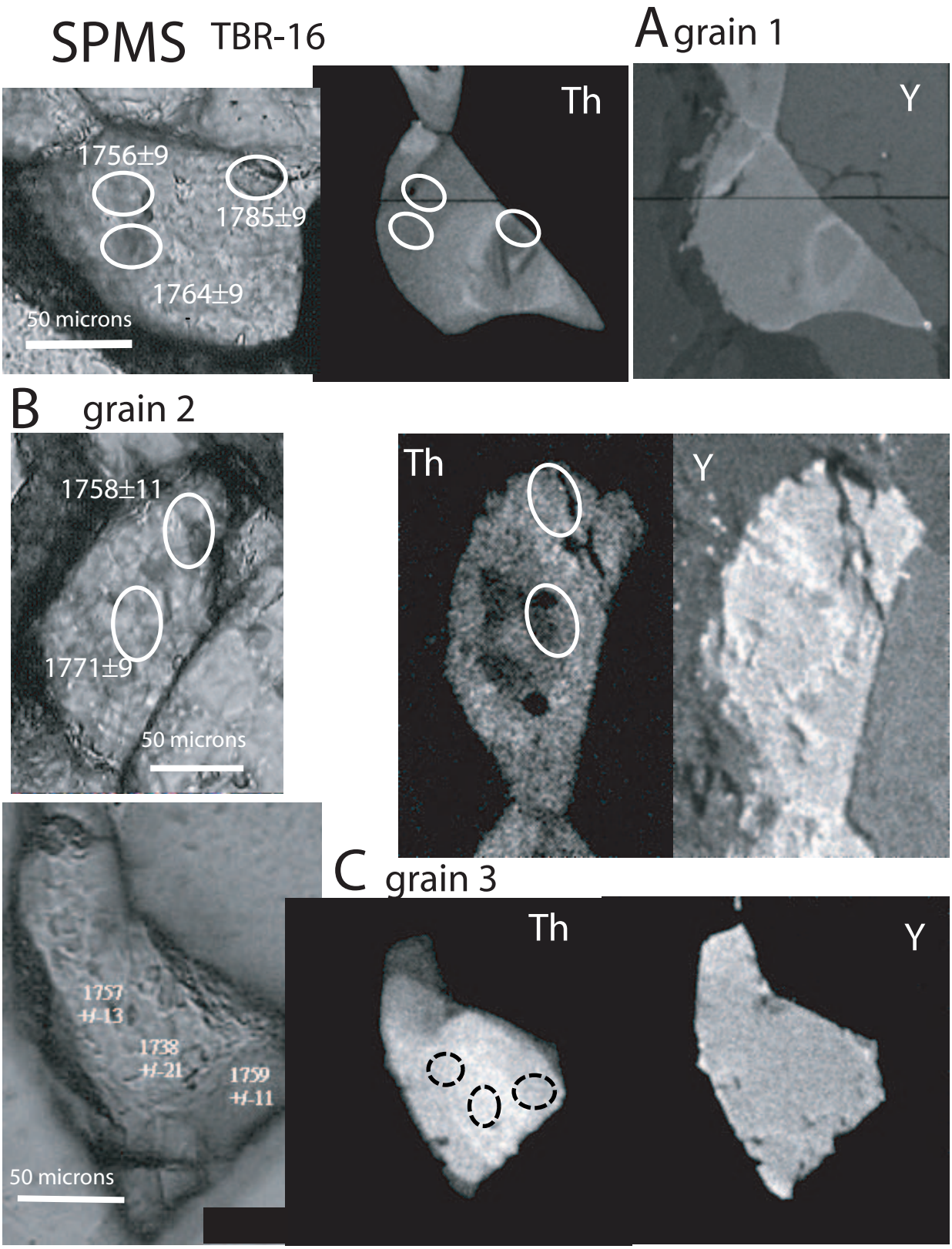
SPMS TBR-16
A grain 1
1756±9
1785±9
1764±9
50 microns
Th
Y
B grain 2
1758±11
1771±9
50 microns
Th
Y
1757
+/-13
1738
+/-21
1759
+/-11
50 microns
C grain 3
Th
Y

PMMMS

JBB-27b

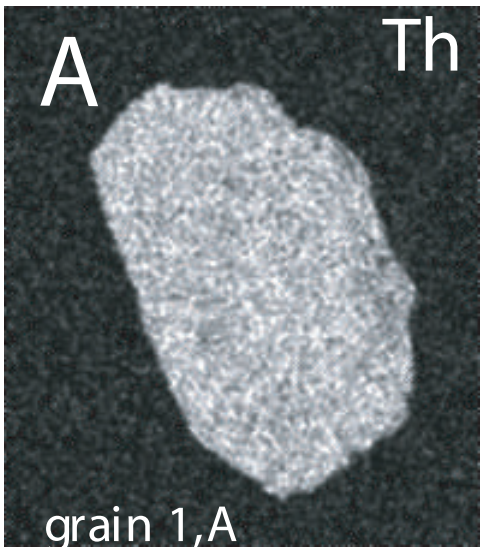

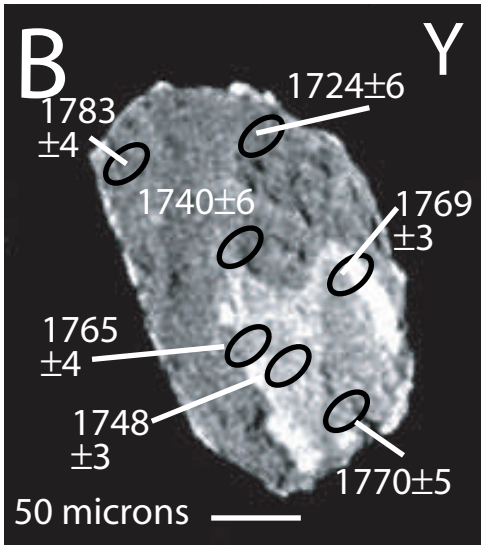

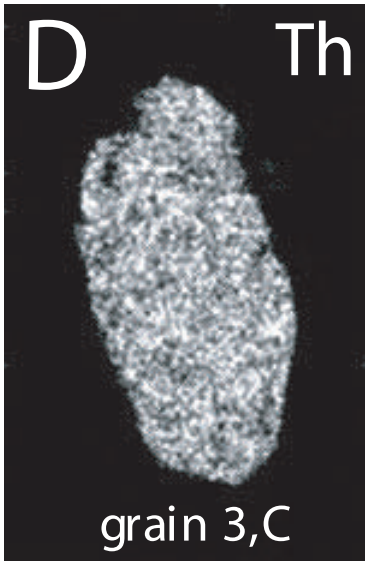

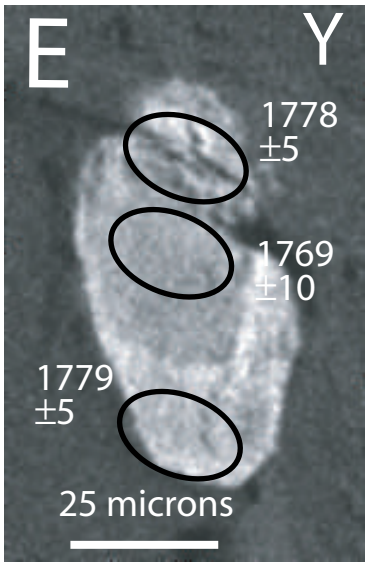

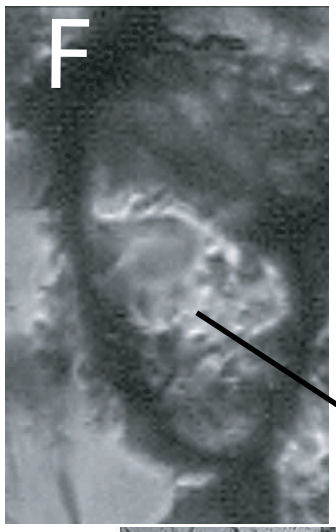

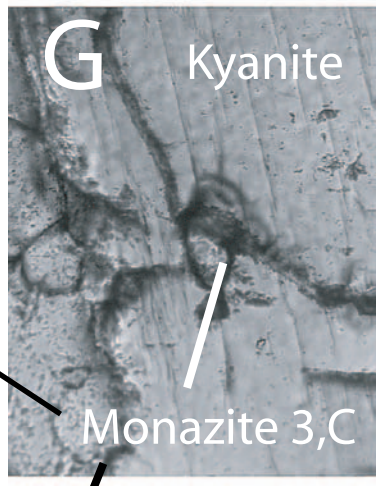

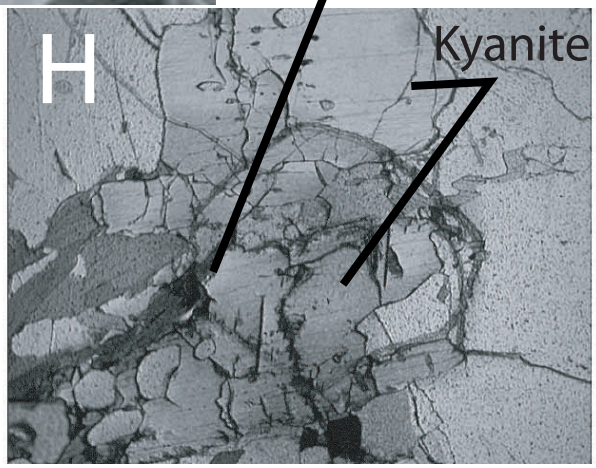

PMMMS

TBR-208 Grain A

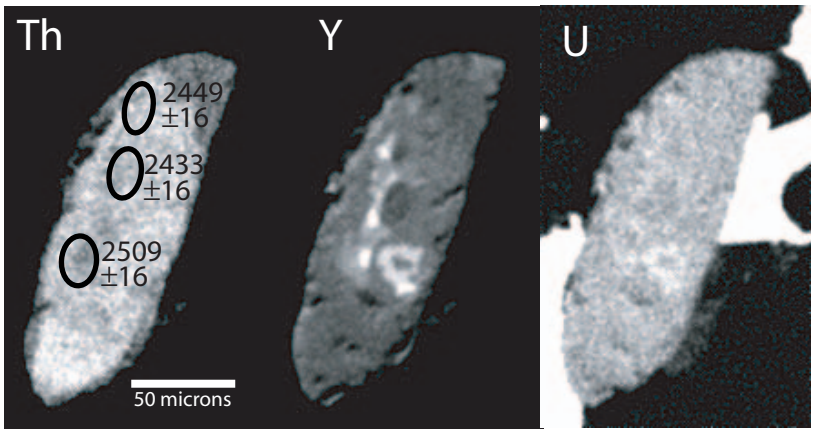

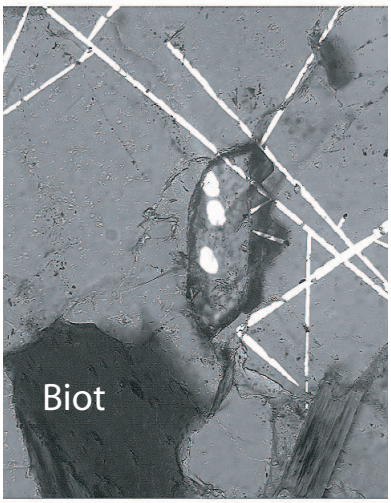

TBR-208 Grain B

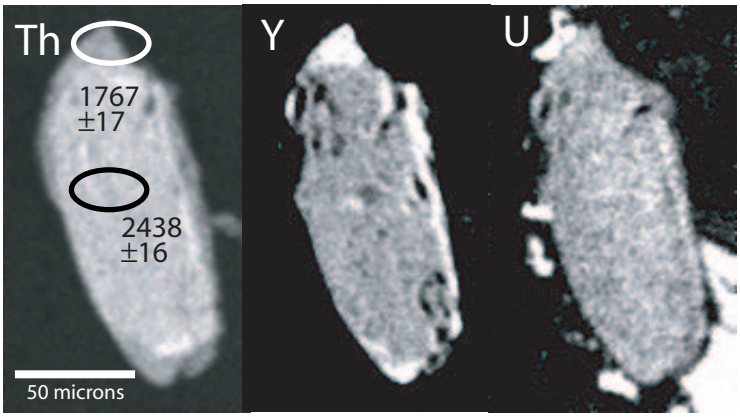

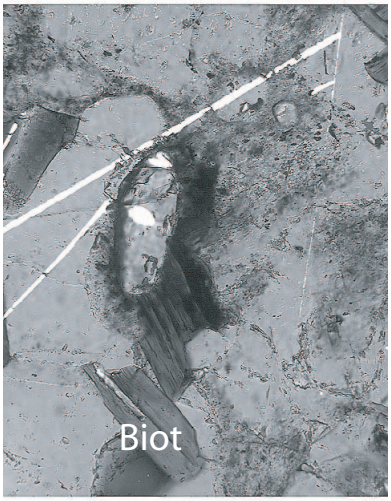

TBR-208 Grain C

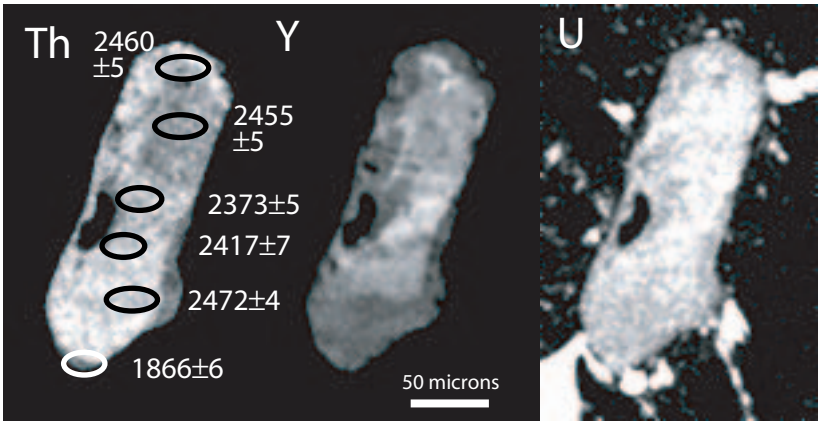

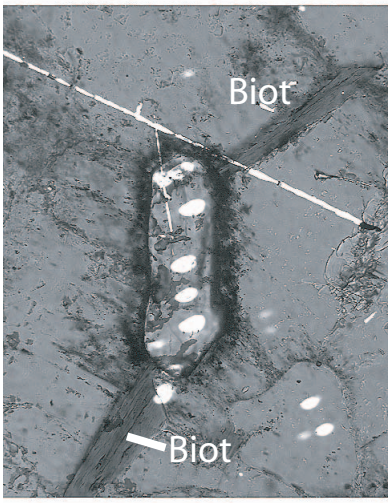

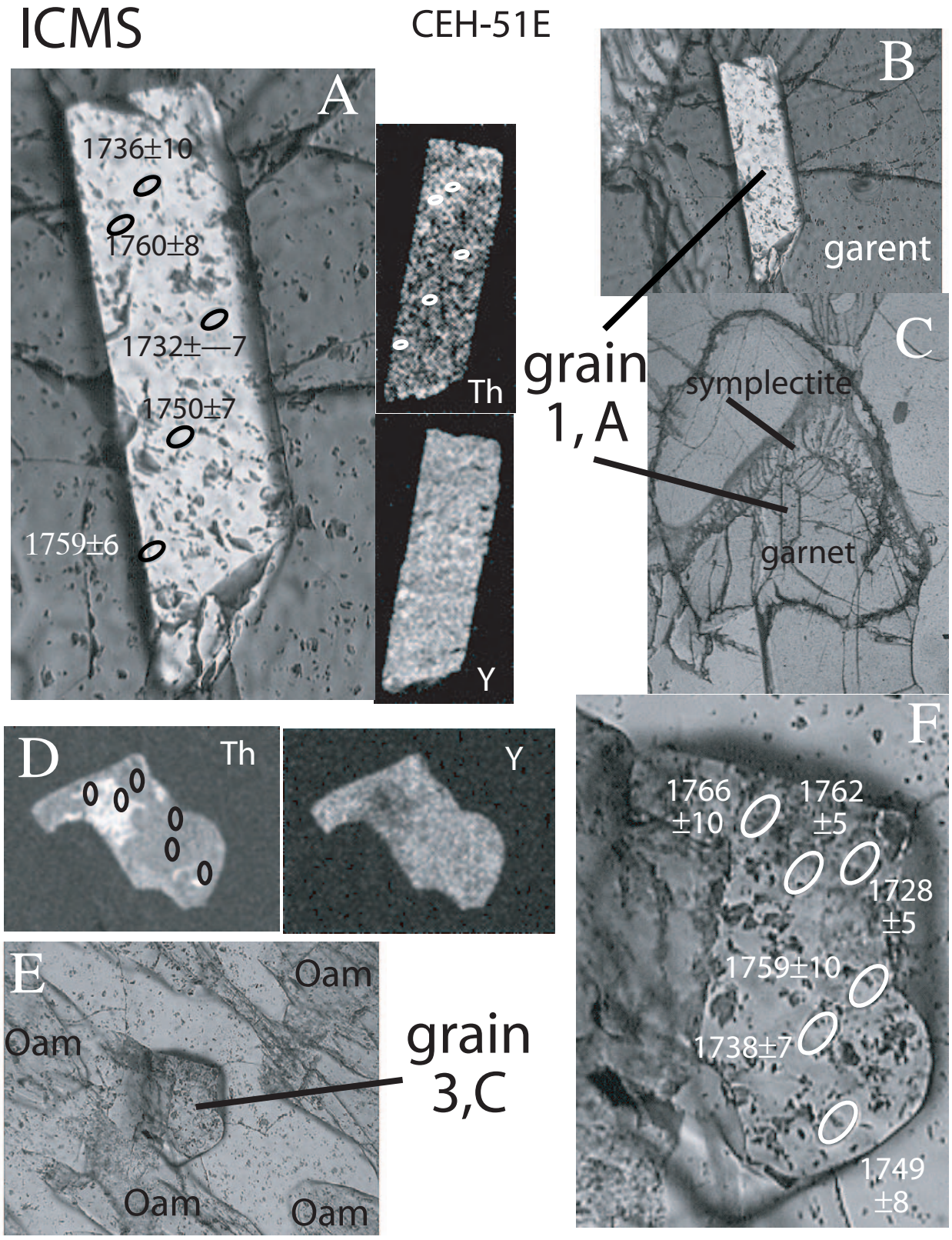
ICMS
CEH-51E
A
1736±10
1760±8
1732±—7
1750±7
1759±6
Th
Y
B
garent
grain
1, A
C
symplectite
garnet
D
Th
Y
E
Oam
Oam
Oam
Oam
grain
3,C
F
1766
±10
1762
±5
1728
±5
1759±10
1738±7
1749
±8

ICMS TBR-83a

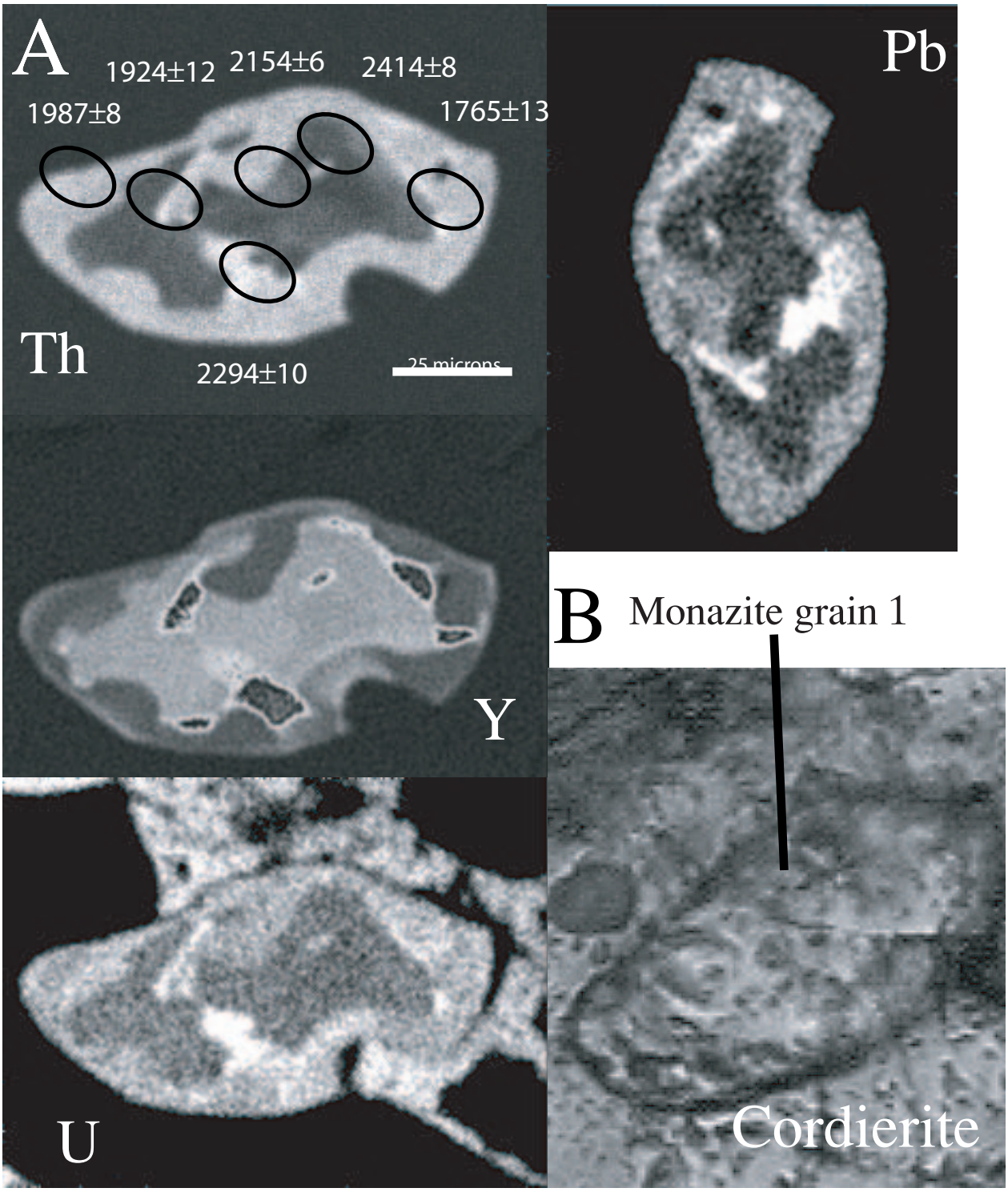
A
1924±12
2154±6
2414±8
1987±8
1765±13
Th
2294±10
25 microns
Pb
Y
B
Monazite grain 1
U
Cordierite

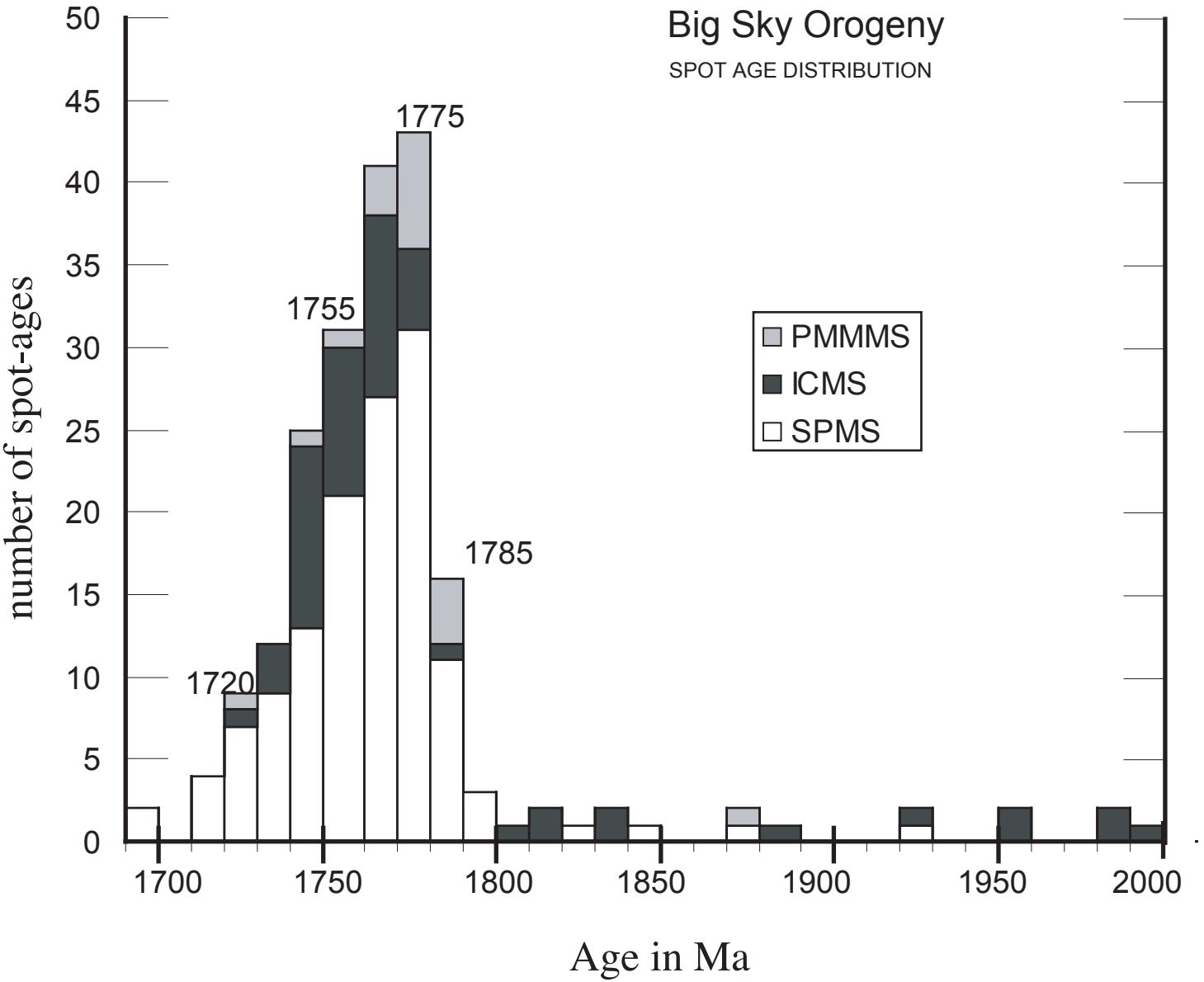
Big Sky Orogeny
SPOT AGE DISTRIBUTION
number of spot-ages
Age in Ma
PMMMS
ICMS
SPMS
1720
1755
1775
1785
0
5
10
15
20
25
30
35
40
45
50
1700
1750
1800
1850
1900
1950
2000

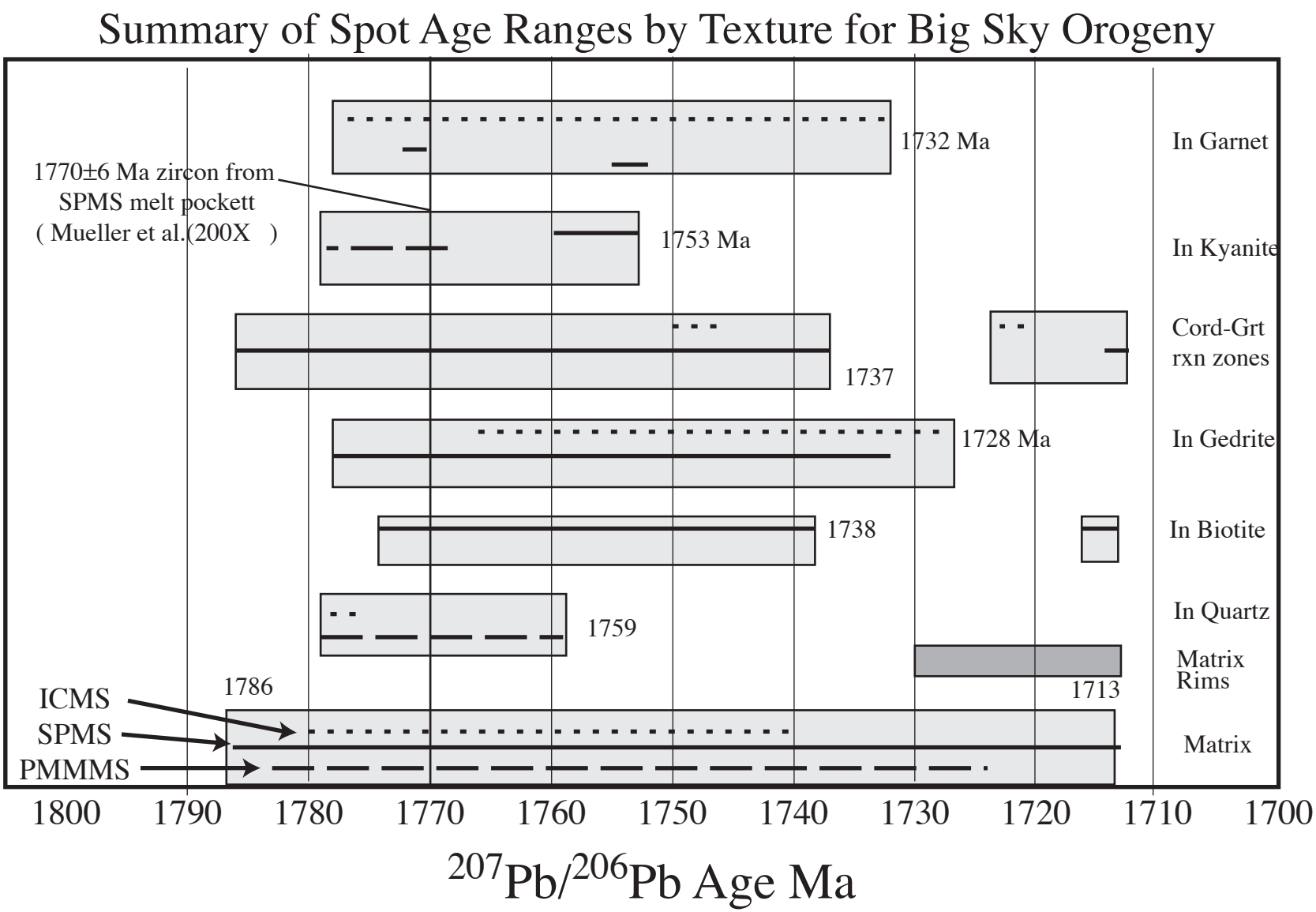
Summary of Spot Age Ranges by Texture for Big Sky Orogeny
1770±6 Ma zircon from
SPMS melt pockett
(Mueller et al.(200X)
1732 Ma
In Garnet
1753 Ma
In Kyanite
1737
Cord-Grt
rxn zones
1728 Ma
In Gedrite
1738
In Biotite
1759
In Quartz
1786
1713
Matrix
Rims
ICMS
SPMS
PMMMS
Matrix
1800
1790
1780
1770
1760
1750
1740
1730
1720
1710
1700
207Pb/206Pb Age Ma

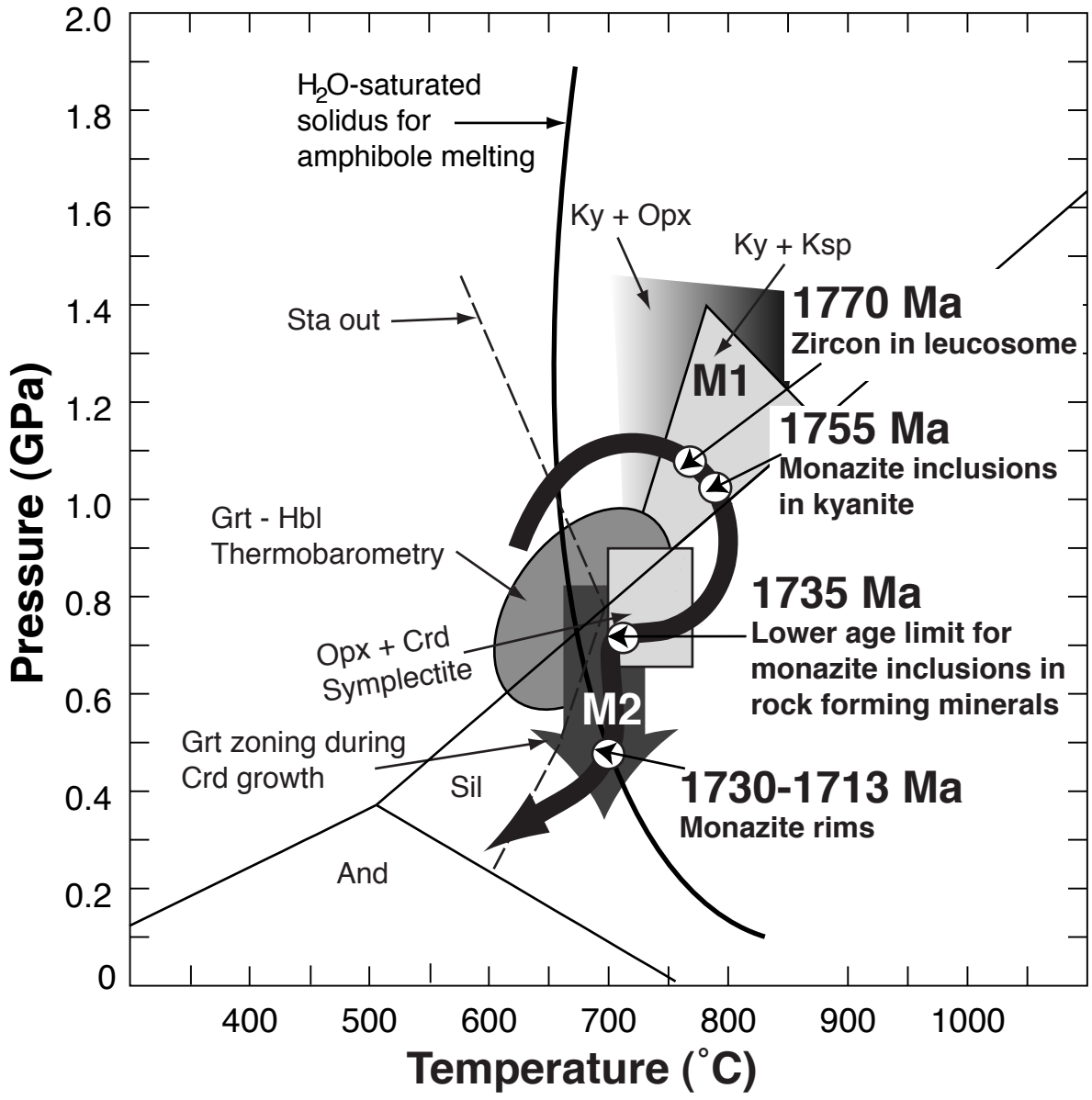
2.0
1.8
1.6
1.4
1.2
1.0
0.8
0.6
0.4
0.2
0
Pressure (GPa)
400
500
600
700
800
900
1000
Temperature (˚C)
H2O-saturated
solidus for
amphibole melting
Ky + Opx
Ky + Ksp
Sta out
1770 Ma
Zircon in leucosome
M1
1755 Ma
Monazite inclusions
in kyanite
Grt - Hbl
Thermobarometry
1735 Ma
Lower age limit for
monazite inclusions in
rock forming minerals
Opx + Crd
Symplectite
M2
Grt zoning during
Crd growth
Sil
1730-1713 Ma
Monazite rims
And